RECEIVER ALGORITHM FOR LTE DOWNLINK

AND

KALMAN FILTER FOR SUN POSITION ESTIMATION

A Project Report

submitted by

M. RAJ ANUP

in partial fulfilment of the requirements
for the award of the degree of

MASTER OF TECHNOLOGY

DEPARTMENT OF ELECTRICAL ENGINEERING

INDIAN INSTITUTE OF TECHNOLOGY, MADRAS.

MAY 2014

THESIS CERTIFICATE

This is to certify that the project report titled **RECEIVER ALGORITHM FOR LTE DOWNLINK AND KALMAN FILTER FOR SUN POSITION ESTIMATION**, submitted by **M. Raj Anup**, to the Indian Institute of Technology, Madras, for the award of the degree of **Master of Technology**, is a bona fide record of the project work done by him under my supervision. The contents of this project report, in full or in parts, have not been submitted to any other Institute or University for the award of any degree or diploma.

Dr. R. David Koilpillai
Professor
Dept. of Electrical Engineering
IIT-Madras, 600 036

Place: Chennai
Date: 16/05/2014

ACKNOWLEDGEMENTS

I would like to thank my project guide, Prof. R. David Koilpillai, whose patient and conscientious guidance kept the project on track, interesting and invigorating at all times. I truly appreciate and value his esteemed guidance and encouragement from the beginning to the end of this thesis. I am indebted to him for having helped me to shape the problem and providing insights towards the solution.

I would also like to thank my colleagues: Istdeo Singh, Varughese Mathew and Sharanya, whose interactions served to improve and inspire at every turn.

I sincerely acknowledge the inspiration provided by the IITM Satellite team members: Susurla Suresh and Akshay Gulati, who played substantial roles in motivating and defining this project.

I would like to thank all whose direct and indirect support helped me completing my thesis in time.

Lastly and most importantly, I would like to thank my family: my father, mother and relatives, whose perpetual moral support, advice, encouragement and relentless good cheer have been a constant support for as long as I can remember.

ABSTRACT

KEYWORDS: Channel-Shortening; Widely-Linear filtering; Kalman filtering

Part-I aims at designing a receiver algorithm for Long Term Evolution (LTE) Downlink systems.
Part-II demonstrates the application of the Kalman filtering algorithm for the estimation of sun position.

PART-I:

The LTE system employs Orthogonal Frequency Division Multiplexing of carriers in the downlink. OFDM is a Multi-Carrier Modulation (MCM) technique and when used in a MIMO environment, it is possible to achieve high data rates. OFDM is superior to its peer wideband techniques for its ability to provide interference-free communication using cyclic prefix. However, as the user is moving closer to the cell edge, the possibility of the delay spread being greater than cyclic prefix causes Inter OFDM Symbol Interference (IOSI), Inter Block Interference (IBI) etc. Further, interference from other base stations might pave way to Co-Channel Interference (CCI) and Co-Antenna Interference (CAI) (due to Multiple Input Multiple Output (MIMO)). In addition, OFDM system is highly sensitive to frequency offset, thus leading to Inter Carrier Interference (ICI). A method referred to as Channel-Shortening is introduced to overcome these interference problems via linear filtering and increasing the number of receive antennas. In this thesis, a new method is proposed that exhibits merits

of Channel-Shortening but with reduced number of receive antennas. The proposed method is simulated and the results are compared with those of the traiditional channel-shortening method.

PART-II:

Spacecrafts require information regarding their orientation with respect to the sun. The estimation of sun's position is corrupted due to the presence of uncontrollable noise sources and impairements. Hence, a robust filtering mechanism is of utmost importance to locate the sun in the presence of measurement noise. In this thesis, two types of sun orientation sensors, namely Tetra-lateral and Pin-cushion are studied. These approaches use the Kalman filter for robust estimation. The results thus obtained, are compared with those of algebraic (Least Squares) method.

TABLE OF CONTENTS

LIST OF TABLES

LIST OF FIGURES

ABBREVIATIONS

LTE	**L**ong **T**erm **E**volution
UMTS	**U**niversal **M**obile **T**elecommunications **S**ystem
HSPA	**H**igh **S**peed **P**acket **A**ccess
OFDM	**O**rthogonal **F**requency **D**ivision **M**ultiplexing
MIMO	**M**ultiple **I**nput **M**ultiple **O**utput
IOSI	**I**nter **O**FDM **S**ymbol **I**nterference
IBI	**I**nter **B**lock **I**nterference
CCI	**C**o-**C**hannel **I**nterference
CAI	**C**o-**A**ntenna **I**nterference
ICI	**I**nter **C**arrier **I**nterference
PSD	**P**osition **S**ensitive **D**evice/**D**etector

CHAPTER 1

INTRODUCTION

1.1 Receiver Algorithm

1.1.1 Introduction

The ever increasing demand for very high rate wireless data transmission calls for technologies which make use of the available electromagnetic resource in the most intelligent way. Key objectives are spectrum efficiency (bits per second per Hertz), robustness against multipath propagation, range, power consumption, and implementation complexity. These objectives are often conflicting, so techniques and implementations are sought which offer the best possible trade-off between them. The Internet revolution has created the need for wireless technologies that can deliver data at high speeds in a spectrally efficient manner. The significant need for higher data rate has pushed wireless communication from 3G to evolution of 4G. Standards of 4G being LTE and WiMAX.

LTE, an acronym for Long-Term Evolution, commonly marketed as 4G LTE, is a standard for wireless communication of high-speed data for mobile phones and data terminals. LTE, the successor to UMTS and HSPA, is now being deployed and is the way forwards for high speed cellular services. The standard is developed by the 3GPP (3rd Generation Partnership Project) and is specified in its Release 8 document series, with minor enhancements described in Release 9 (**[19]**). In its first form it is a 3G or as

some would call it a 3.99G technology, but with further additions the technology can be migrated to a full 4G standard and here it is known as LTE Advanced. There has been a rapid increase in the use of data carried by cellular services, and this increase will only become larger in what has been termed the "data explosion". To cater for this and the increased demands for increased data transmission speeds and lower latency, further development of cellular technology have been required.

The UMTS cellular technology upgrade has been dubbed LTE. The idea is that LTE will enable much higher speeds to be achieved along with much lower packet latency (a growing requirement for many services these days), and that 3GPP LTE will enable cellular communications services to move forward to meet the needs for cellular technology to 2017 and well beyond. Many operators have not yet upgraded their basic 3G networks, and 3GPP LTE is seen as the next logical step for many operators, who will leapfrog straight from basic 3G straight to LTE as this will avoid providing several stages of upgrade. The use of LTE will also provide the data capabilities that will be required for many years and until the full launch of the full 4G standards known as LTE Advanced.

The goal of LTE was to increase the capacity and speed of wireless data networks using new DSP (digital signal processing) techniques and modulations that were developed around the turn of the millennium. Orthogonal Frequency Division Multiplexing (OFDM) is one such promising technique and is being effectively exploited. A further goal was the redesign and simplification of the network architecture to an IP-based system with significantly reduced transfer latency compared to the 3G architecture. The LTE wireless interface is incompatible with 2G and 3G networks, so that it must be operated on a separate wireless spectrum.

OFDM is the potential candidate for LTE systems. It can provide large data rates with sufficient robustness to radio channel impairments. The major advantages of OFDM are its ability to convert a frequency selective fading channel into several nearly flat fading channels and high spectral efficiency. One of the disadvantages is its high Peak-to-

Average Power Ratio (PAPR) which imposes a severe constraint on transmitter power. Hence it is used only in the downlink part of the LTE systems. For the uplink case, Single Carrier- Frequency Division Multiple Access (SC-FDMA) is used. The other disadvantage is its sensitivity to carrier frequency offset which results in ICI. ICI combined with other drawbacks such as IOSI , IBI , CCI, CAI will degrade the performance of the system.

1.1.2 Motivation

Orthogonal Frequency Division Multiple Access(OFDMA) is the technique used in LTE Downlink systems. OFDM is robust in adverse channel conditions and allows a high level of spectral efficiency. Multiple access techniques which are quite developed for the single carrier modulations (e.g. TDMA, FDMA) had made possible of sharing one communication medium by multiple number of users simultaneously. The sharing is required to achieve high capacity by simultaneously allocating the available bandwidth to multiple users without severe degradation in the performance of the system. Disadvantage of FDMA technique is its Bad Spectrum Usage. Disadvantage of TDMA technique is Multipath Delay spread problem. In a typical terrestrial broadcasting, the transmitted signal arrives at the receiver using various paths of different lengths. Since multiple versions of the signal interfere with each other, it becomes difficult to extract the original information.

OFDM has recently gained fair degree of prominence among modulation schemes due to its intrinsic robustness to frequency selective Multipath fading channels. OFDM system also provides higher spectrum efficiency and supports high data rate transmission. This is one of the main reasons to select OFDM a candidate for systems such as Digital Audio Broadcasting (DAB), Digital Video Broadcasting (DVB), Digital Subscriber Lines (DSL), and Wireless local area networks (HiperLAN/2), and in IEEE 802.11a, IEEE 802.11g.

The focus of fourth-generation (4G) mobile systems is on supporting high data rate services such as deployment of multi-media applications which involve voice, data, pictures, and video over the wireless networks. The data rate envisioned for 4G networks is 1 GB/s for indoor and 100Mb/s for outdoor environments. OFDM is a promising candidate for 4G systems because of its robustness to the multipath environment. But because of its high Peak-to-Average Power Ratio (PAPR), it is used only in the downlink and SC-FDMA is used in the uplink part.

The most commonly encountered problems in OFDM are:

- Inter OFDM Symbol Interference (IOSI)
- Inter Block Interference (IBI)
- Co-channel Interference (CCI)
- Co-Antenna Interference (CAI)
- Inter Carrier Interference (ICI)

To specify in particular, OFDM is very sensitive to carrier synchronization and even a small percentage of carrier frequency offset results in huge degradation in performance. Therefore, proposing a technique that is superior to Channel Shortening method in solving these problems, has been my chief focus.

1.1.3 Literature Survey

In 1971, Weinstein and Ebert, engineers at BELL Telephone Laboratories, proposed a modified OFDM system in the paper "**Data Transmission by Frequency Division Multiplexing using the Discrete Fourier Transform**" (**[8]**). The paper demonstrated use of Discrete Fourier Transform (DFT) to generate the orthogonal subcarriers waveforms as a substitute to banks of sinusoidal generators. Use of DFT and IDFT modules alongside with digital-to-analog converters immensely reduced implementation complexity. In their model, baseband signals were modulated by exercising IDFT at the

transmitter end and demodulated by DFT at the receiver end. Hence, though the subcarriers overlap in frequency domain, DFT ensured their orthogonality.

Cyclic prefix (CP) or cyclic extension was first introduced by Peled and Ruiz in 1980 for OFDM systems. They suggested substitution of conventional null guard interval with cyclic extension for fully-loaded OFDM modulation. This ensured persistence of orthogonality between subcarriers, hence resulting in phenomenal Inter Symbol Interference (ISI) reduction. However, decline in transmitting energy efficiency, innate in this process, is the price to pay. For its merits, Cyclic Prefix is being adopted by current IEEE standards.

In 1985, Cimini introduced a pilot-based method to reduce the interference emanating from the multipath and co-channels. In the 1990s, OFDM systems have been exploited for high data rate communications. In the IEEE 802.11 standard, the carrier frequency can go up as high as 2.4 GHz or 5 GHz. Researchers tend to pursue OFDM operating at even much higher frequencies nowadays. For example, the IEEE 802.16 standard proposes yet higher carrier frequencies ranging from 10 GHz to 60 GHz. However, OFDM is very sensitive to the carrier frequency offsets which causes Inter Carrier Interference (ICI). The undesired ICI degrades the performance of the OFDM systems. The use of channel-shortening method for removal of ICI was introduced by Robert W. Heath and Taiwan Tang in their paper "**A Space-Time Receiver with Joint Synchronization and Interference Cancellation in Asynchronous MIMO-OFDM Systems**".

1.1.4 Contribution of this thesis

Using MATLAB, simulations were carried out for the Proposed method and Channel-Shortening method. Digital modulation schemes such as 4-QAM and 16-QAM were used to assess the performance of the proposed method. Bit-error-rate (BER) for varying Signal-to-Noise Ratio (SNR) is used to compare the Proposed method against the traditional Channel-Shortening method and the added advantages offered by it are high-

lighted. Different MIMO scenarios were taken and performance of the proposed method against IOSI, IBI, CAI, CCI, ICI (due to frequency offset) is discussed.

1.2 Kalman Filter Algorithm

1.2.1 Introduction

The Kalman filter is a recursive predictive filter that is based on the use of state space techniques and recursive algorithms. It estimates the state of a dynamic system. This dynamic system can be disturbed by various noises, mostly assumed to be white. To improve the estimated state the Kalman filter uses measurements that are related to the state but disturbed profusely.

The algorithm works in a two-step process. In the prediction step, the Kalman filter produces estimates of the current state variables, along with their uncertainties. Once the outcome of the next measurement (necessarily corrupted with some amount of error, including random noise) is observed, these estimates are updated using a weighted average, with more weight being given to estimates with higher certainty. Because of the algorithm's recursive nature, it can run in real time using only the present input measurements and the previously calculated state and its uncertainty matrix; no additional past information is required.

The major advantages of using Kalman filter for the estimation of data is that it copes with the large uncertainty of the initialization phase, copes with missing data and provides a convenient measure of estimation accuracy (via the covariance matrix). However, it is computationally complex and requires linear models for state dynamics and observation processes.

1.2.2 Motivation

Many satellites use sun sensors to determine the position of the sun which can be further used for various other purposes such as attitude determination, alignment towards sun for solar charging, etc. All these applications require perfect position of the sun (elevation and azimuth angles of the sun with respect to sensor frame). The position estimates from the sun sensor will be, in general, erroneous because of the various noises that may affect the measurements. Some of these noises may be random in nature. Hence to have a robust estimate of the sun position , there must be a filtering mechanism through which the sun sensor output data must pass so that the filtered output would be the best estimate of the sun position. Kalman Filter has been chosen in this project for it considers approximately all noise sources that might affect the sensor output, thus giving a robust estimate of the sun's position.

1.2.3 Literature Survey

Rudolf Emil Kalman was born in Budapest, Hungary, on May 19, 1930. He envisioned Kalman filter for the first time in the year 1958. In 1960, he published his famous paper describing a recursive solution to the discrete data linear filtering problem. Since that time, due to advances in digital computing, the Kalman filter has been the subject of extensive research and application, particularly in the area of autonomous or assisted navigation. This digital filter is sometimes called the Stratonovich–Kalman–Bucy filter because it is a special case of a more general, non-linear filter developed somewhat earlier by the Soviet mathematician Ruslan L. Stratonovich. In fact, some of the special case linear filter's equations appeared in papers by Stratonovich that were published before summer 1960, when Kalman met with Stratonovich during a conference in Moscow.

1.2.4 Contribution of this thesis

Simulations were carried out in MATLAB, where the kalman filtering algorithm is run iteratively. The algorithm was tested on two sun sensor types namely pin-cushion type and tetra-lateral type. Results were compared with those of algebraic method (Least-Squares).

1.3 Objective and Outline of the Thesis

The main objective of the thesis can be given as:

1. To propose a method which could outperform the Channel-Shortening method and provide a better diversity advantage along with other advantages of the Channel-Shortening method.
2. To implement the kalman filtering algorithm for robust estimation of the sun position from sun sensor data and prove that this is a powerful tool compared to the other traditional methods (in particular least squares method).

This thesis is organized as follows:

We begin, in Chapter-2, by elaborating basics of LTE and OFDM systems. Chapter-3 demonstrates the Channel-Shortening method which is used for removal of IOSI, IBI, CCI, CAI, ICI, etc. In Chapter-4, the Proposed method which uses the concept of widely-linear filtering is discussed. Chapter-5 presents the theoretical and simulation results of the Proposed method against Channel-Shortening method.

Chapter-6 delineates various types of sun sensors and introduces the Kalman Filtering algorithm. Chapter-7 elucidates the estimation of the sun position using Kalman Filtering algorithm. Chapter-8 is a presentation of simulation results of the Kalman Filtering algorithm. In addition, the chapter brings out superiority of the algorithm to least squares method. Chapter-9 concludes the thesis and gives scope for future work.

RECEIVER ALGORITHM FOR LTE DOWNLINK

CHAPTER 2

BASICS OF LTE AND OFDM

2.1 LTE Systems

History

LTE stands for Long Term Evolution and it was initiated as a project in 2004 by telecommunication body known as the Third Generation Partnership Project (3GPP). LTE evolved from an earlier 3GPP system known as the Universal Mobile Telecommunication System (UMTS), which in turn evolved from the Global System for Mobile Communications (GSM). First version of LTE was documented in Release 8 of the 3GPP specifications. System Architecture Evolution (SAE) is the corresponding evolution of the GPRS/3G packet core network evolution. The term LTE is typically used to represent both LTE and SAE. Table 2.1.1 illustrates the evolution of LTE.

Year	Event
Mar 2000	Release99-UMTS/WCDMA
Mar 2002	Release5-HSDPA
Mar 2005	Release6-HSUPA
2007	Release7-DL MIMO, IMS (IP Multimedia Subsystem)
Nov 2004	Work started on LTE Specification
Jan 2008	Spec finalized and approved with Release8
2010	Targeted first deployment

Table 2.1.1: LTE Evolution adapted from **[17]**

Specifications of LTE

Table 2.1.2 summarizes the basic parameters of LTE systems.

Parameters	Description
Frequency range	UMTS FDD and TDD bands as given in Table 2.1.3
Duplexing	FDD, TDD, half-duplex FDD
Channel coding	Turbo code
Mobility	0-15 km/h (optimized) 15-120 km/h (high performance)
Channel Bandwidth (MHz)	1.4, 3, 5, 10, 15, 20
Modulation Schemes	UL : QPSK, 16QAM, 64QAM (optional) DL : QPSK, 16QAM, 64QAM
Multiple Access schemes	UL: SC-FDMA (Single Carrier Frequency Division Multiple Access) supports 50Mbps+ (20MHz spectrum) DL: OFDM (Orthogonal Frequency Division Multiple Access) supports 100Mbps+ (20MHz spectrum)
Multi-Antenna Technology	UL : Multi-user Collaborative MIMO DL: TxAA, spatial multiplexing, CDD ,max 4x4 array
Peak data rate in LTE	UL: 75Mbps(20MHz bandwidth) DL: 150Mbps(2x2 MIMO, 20MHz bandwidth) 300Mbps(4x4 MIMO, 20MHz bandwidth)
MIMO	UL: 1 x 2, 1 x 4 DL: 2 x 2, 4 x 2, 4 x 4
Coverage	5 - 100km with slight degradation after 30km
QoS	E2E QOS allowing prioritization of different class of service
Latency	End-user latency < 10mS

Table 2.1.2: Specifications of LTE adapted from [**17**]

LTE uses wide variety of bandwidth allocations or radio spectrum that has been reserved for FDD, frequency division duplex, and TDD, time division duplex. The FDD LTE frequency bands are paired to allow simultaneous transmission on two frequencies. The TDD LTE bands are unpaired as the uplink and downlink share the same frequency, being time multiplexed.

Table 2.1.3 gives the frequency band allocation for LTE FDD and TDD systems.

FDD					
LTE Band no.	**Uplink (MHz)**	**Downlink (MHz)**	**Width of band (MHz)**	**Duplex spacing (MHz)**	**Band gap (MHz)**
1	1920 - 1980	2110 - 2170	60	190	130
2	1850 - 1910	1930 - 1990	60	80	20
3	1710 - 1785	1805 -1880	75	95	20
4	1710 - 1755	2110 - 2155	45	400	355
5	824 - 849	869 - 894	25	45	20
6	830 - 840	875 - 885	10	35	25
7	2500 - 2570	2620 - 2690	70	120	50
8	880 - 915	925 - 960	35	45	10
9	1749.9 - 1784.9	1844.9 - 1879.9	35	95	60
10	1710 - 1770	2110 - 2170	60	400	340
11	1427.9 - 1452.9	1475.9 - 1500.9	20	48	28
12	698 - 716	728 - 746	18	30	12
13	777 - 787	746 - 756	10	-31	41
14	788 - 798	758 - 768	10	-30	40
15	1900 - 1920	2600 - 2620	20	700	680
16	2010 - 2025	2585 - 2600	15	575	560
17	704 - 716	734 - 746	12	30	18
18	815 - 830	860 - 875	15	45	30
19	830 - 845	875 - 890	15	45	30
20	832 - 862	791 - 821	30	-41	71
21	1447.9 - 1462.9	1495.5 - 1510.9	15	48	33
22	3410 - 3500	3510 - 3600	90	100	10
23	2000 - 2020	2180 - 2200	20	180	160
24	1625.5 - 1660.5	1525 - 1559	34	-101.5	135.5
25	1850 - 1915	1930 - 1995	65	80	15

TDD		
LTE Band no.	**Allocation (MHz)**	**Width of band (MHz)**
33	1900 - 1920	20
34	2010 - 2025	15
35	1850 - 1910	60
36	1930 - 1990	60
37	1910 - 1930	20
38	2570 - 2620	50
39	1880 - 1920	40
40	2300 - 2400	100
41	2496 - 2690	194
42	3400 - 3600	200
43	3600 - 3800	200

Table 2.1.3: LTE FDD and TDD frequency band allocations adapted from **[17]**

Advantages of LTE

- **High Throughput** : High data rates can be achieved in both downlink as well as uplink. This causes high throughput.
- **Low Latency :** Time required to connect to the network is in range of a few hundred milliseconds and power saving states can now be entered and exited very quickly.
- **FDD and TDD in the same platform :** Frequency Division Duplex (FDD) and Time Division Duplex (FDD), both schemes can be used on same platform.
- **Superior end-user experience :** Optimized signalling for connection establishment and other air interface and mobility management procedures have further improved the user experience. Reduced latency (to 10 ms) for better user experience.
- **Seamless Connection :** LTE will also support seamless connection to existing networks such as GSM, CDMA and WCDMA.
- **Plug and play :** The user does not have to manually install drivers for the device. Instead system automatically recognizes the device, loads new drivers for the hardware if needed, and begins to work with the newly connected device.
- **Simple architecture :** Because of Simple architecture low operating expenditure (OPEX).

2.2 OFDM Systems

To overcome the effect of multi path fading problem available in UMTS, LTE uses Orthogonal Frequency Division Multiplexing (OFDM) for the downlink - that is, from the base station to the terminal to transmit the data over many narrow band careers of 180 KHz each instead of spreading one signal over the entire channel bandwidth.

Orthogonal Frequency Division Multiplexing (OFDM) is a multicarrier transmission technique, which divides the bandwidth into many carriers, each one is modulated by a low rate data stream(see Figure 2.2.1). In term of multiple access technique, OFDM is similar to FDMA in that the multiple user access is achieved by subdividing the available bandwidth into multiple channels that are then allocated to users. However,

OFDM uses the spectrum much more efficiently by spacing the channels much closer together. This is achieved by making all the carriers orthogonal to one another, hence preventing interference between the carriers though closely spaced.

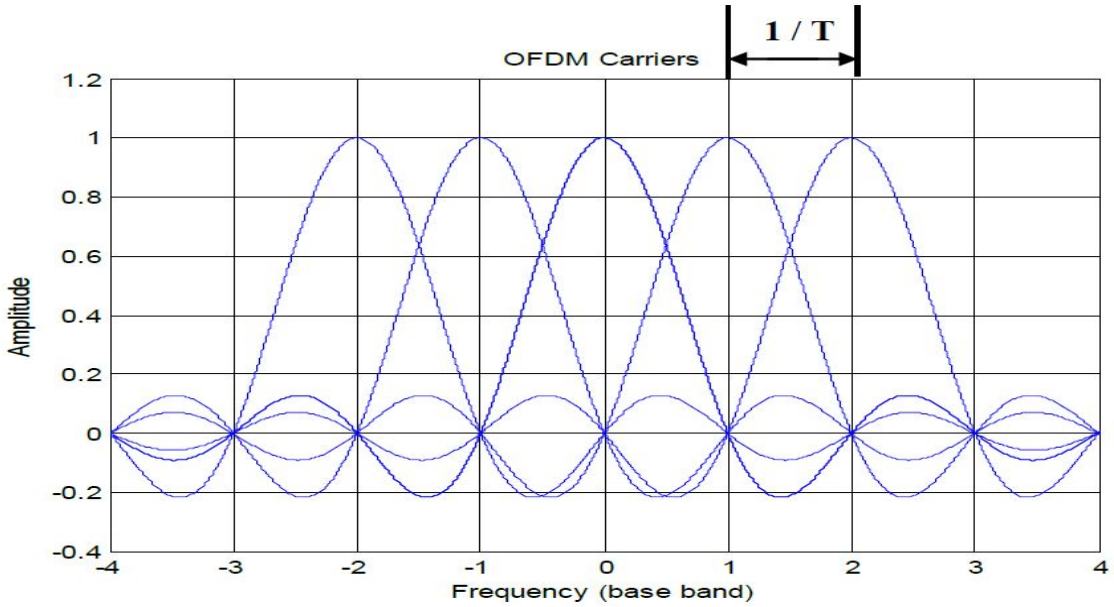

Figure 2.2.1: OFDM Spectrum

2.2.1 Evolution of OFDM

The evolution of OFDM can be divided into three parts namely Frequency Division Multiplexing (FDM), Multicarrier Communication (MC) and Orthogonal Frequency Division Multiplexing (OFDM).

Frequency division Multiplexing (FDM)

Frequency Division Multiplexing (FDM) was used for a long time to carry more than one signal over a telephone line. FDM enables use of different frequency channels to carry the information of different users. Each channel is identified by the centre frequency of transmission. To ensure that the signal of one channel did not overlap with the signal from an adjacent one, some gap or guard band is introduced between different

channels. Obviously, this guard band will lead to inefficiencies which were exaggerated in the early days. Lack of digital filtering, those days, made it difficult to filter closely packed adjacent channels.

MultiCarrier Communication (MC)

The concept of multicarrier (MC) communications uses a form of FDM technologies but only between a single data source and a single data receiver. As multicarrier communications was introduced, it enabled an increase in the overall capacity of communications, thereby increasing the overall throughput. Referring to MC as FDM, however, is somewhat misleading since the concept of multiplexing refers to the ability to add signals together. MC is actually the concept of splitting a signal into a number of signals, modulating each of these new signals over its own frequency channel, multiplexing these different frequency channels together in an FDM manner; feeding the received signal via a receiving antenna into a demultiplexer that feeds the different frequency channels to different receivers and combining the data output of the receivers to form the received signal.

Orthogonal Frequency Division Multiplexing (OFDM)

Orthogonal Frequency Division Multiplexing (OFDM) is simply defined as a form of multi-carrier modulation where the carrier spacing is carefully selected so that each subcarrier is orthogonal to the other sub-carriers. Orthogonality can be achieved by carefully selecting the sub-carrier frequencies. One of the ways is to select sub-carrier frequencies such that they are harmonics to each other. Also the modulators and demodulators in MC were replaced by DSP techniques such as IFFT and FFT respectively which reduces the computation effort and time.

2.2.2 OFDM Transmission and Reception

Figure 2.2.2 shows the block diagram of a typical OFDM transceiver. The transmitter section converts digital data to be transmitted, into a mapping of subcarrier amplitude and phase. It then transforms this spectral representation of the data into the time domain using an Inverse Discrete Fourier Transform (IDFT). The Inverse Fast Fourier Transform (IFFT) performs the same operations as an IDFT, except that it is much more computationally efficient, and so is used in all practical systems. In order to transmit the OFDM signal the calculated time domain signal is then mixed up to the required frequency. The receiver performs the reverse operation of the transmitter, mixing the RF signal to base band for processing, then using a Fast Fourier Transform (FFT) to analyze the signal in the frequency domain. The amplitude and phase of the subcarriers is then picked out and converted back to digital data. The IFFT and the FFT are complementary function and the most appropriate term depends on whether the signal is being received or generated. In cases where the signal is independent of this distinction then the term FFT and IFFT is used interchangeably. The high data rate serial input bit stream is fed into serial to parallel converter to get low data rate output parallel bit stream. Input bit stream is taken as binary data. The low data rate parallel bit stream is modulated in Signal Mapper. Modulation can be BPSK, QPSK,QAM etc. The modulated data are served as input to inverse fast Fourier transform so that each subcarrier is assigned with a specific frequency. The frequencies selected are orthogonal frequencies. In IFFT, the frequency domain OFDM symbols are converted into time domain OFDM symbols. Guard interval is introduced in each OFDM symbol to eliminate inter symbol interference (ISI). All the OFDM symbols are taken as input to parallel to serial data. These OFDM symbols constitute a frame. A number of frames can be regarded as one OFDM signal. This OFDM signal is allowed to pass through digital to analog converter (DAC). In DAC the OFDM signal is fed to RF power amplifier for transmission. Then the signal is allowed to pass through channel where Additive White Gaussian Noise (AWGN) also gets added. At the receiver part, the received OFDM

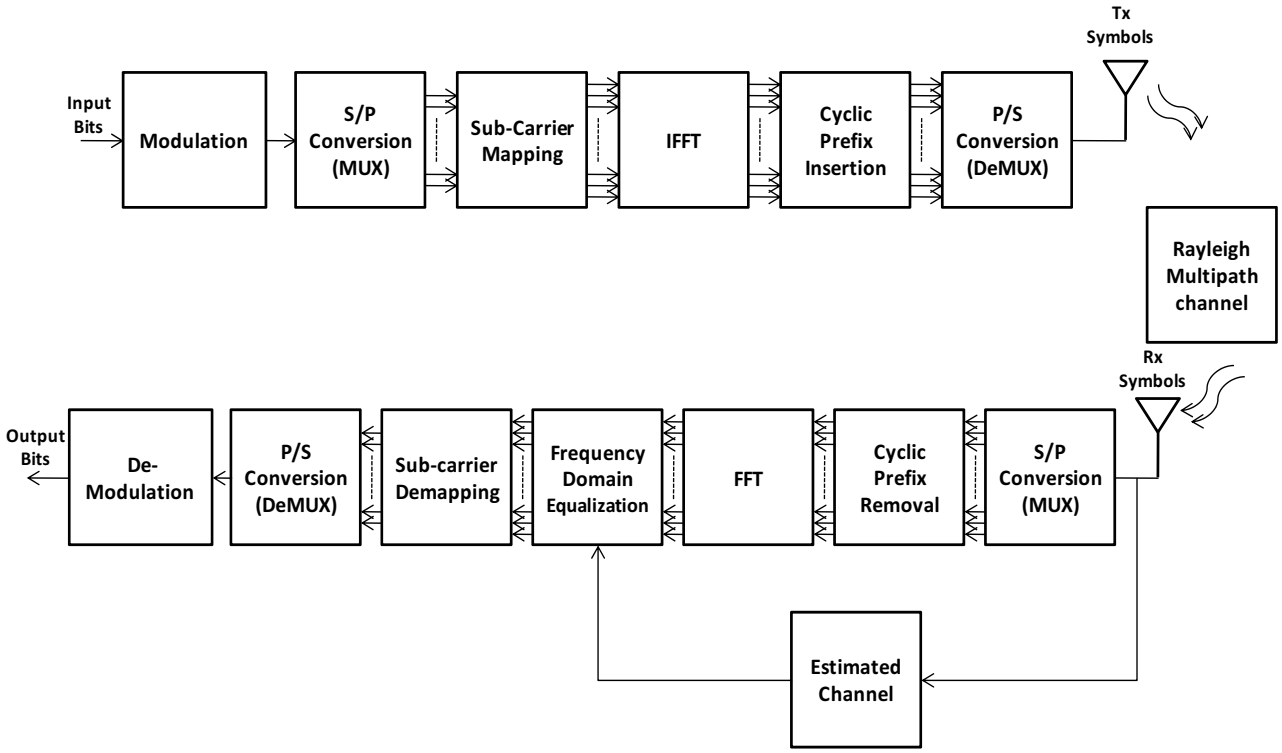

Figure 2.2.2: Basic Block Diagram of OFDM

signal is fed to analog to digital converter (ADC) and is taken as input to serial to parallel converter. In these parallel OFDM symbols, Guard interval is removed and it is allowed to pass through Fast Fourier transform. Here the time domain OFDM symbols are converted into frequency domain. Then it is passed through the frequency domain equalizer (MMSE, ZF, ML, etc) to extract the transmitted symbols and then fed into Signal Demapper for demodulation purpose. And finally the low data rate parallel bit stream is converted into high data rate serial bit stream which is in form of binary.

Advantages and Disadvantages of OFDM

Advantages

- OFDM can easily adapt to severe channel conditions without the need for complex channel equalization algorithms being employed.
- It is robust when combating narrow-band co-channel interference. As only some of the channels will be affected, not all data is lost and error coding can combat this.
- Intersymbol interference, ISI is less of a problem with OFDM because low data rates are carried by each carrier.
- Provides high levels of spectral efficiency.
- Relatively insensitive to timing errors.
- This mechanism also facilitates the design of single frequency networks (SFNs), where several adjacent transmitters send the same signal simultaneously at the same frequency, as the signals from multiple distant transmitters may be combined constructively, rather than interfering as would typically occur in a traditional single-carrier system.

Disadvantages

- OFDM is sensitive to Doppler shift - frequency errors offset the receiver and if not corrected the orthogonality between the carriers is degraded.
- Sensitive to frequency timing issues.
- Possesses a high peak to average power ratio - this requires the use of linear power amplifiers which are less efficient than non-linear ones and this results in higher battery consumption.
- The cyclic prefix used causes a lowering of the overall spectral efficiency.

2.2.3 LTE in Downlink and Uplink

Downlink:

Physical Resource allocation

OFDM meets the LTE requirement for spectrum flexibility and enables cost-efficient solutions for very wide carriers with high peak rates. The basic LTE downlink physical resource can be seen as a time-frequency grid, as illustrated in Figure 2.2.3:

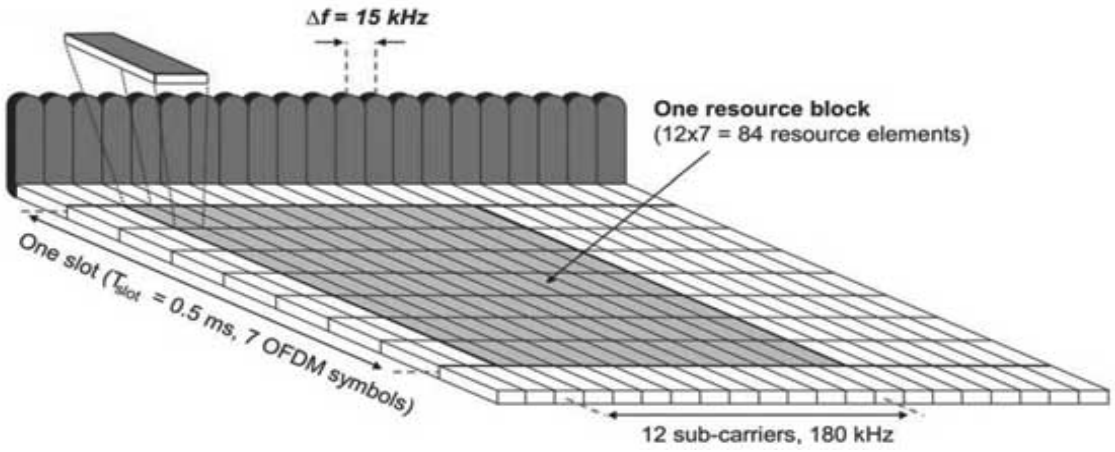

Figure 2.2.3: LTE Downlink Physical Resource allocation adapted from **[17]**

The OFDM symbols are grouped into resource blocks. The resource blocks have a total size of 180KHz in the frequency domain and 0.5ms in the time domain. Each 1ms Transmission Time Interval (TTI) consists of two slots (Tslot). Each user is allocated a number of so-called resource blocks in the time-frequency grid. The more resource blocks a user gets, and the higher the modulation used in the resource elements, the higher the bit-rate. Which resource blocks and how many the user gets at a given point in time depend on advanced scheduling mechanisms in the frequency and time dimensions. The scheduling mechanisms in LTE are similar to those used in HSPA, and enable optimal performance for different services in different radio environments.

Resource blocks comprise 12 subcarriers, regardless of the overall LTE signal bandwidth. They also cover one slot in the time frame. This means that different LTE signal

bandwidths will have different numbers of resource blocks (see Table 2.2.1).

Channel Bandwidth (MHz)	Number of Resource blocks
1.4	6
3	15
5	25
10	50
15	75
20	100

Table 2.2.1: Resource block allocation for each bandwidth adapted from **[18]**

Modulation schemes

Within the OFDM signal it is possible to choose between three types of modulation:

- **QPSK (= 4QAM)** - 2 bits per symbol
- **16QAM** - 4 bits per symbol
- **64QAM** - 6 bits per symbol

The exact format is chosen depending upon the prevailing conditions. The lower forms of modulation (QPSK) do not require such a large signal to noise ratio but are not able to send the data as fast. Only when there is a sufficient signal to noise ratio can the higher order modulation format be used.

Figure 2.2.4 shows the Basic OFDM transmission scheme:

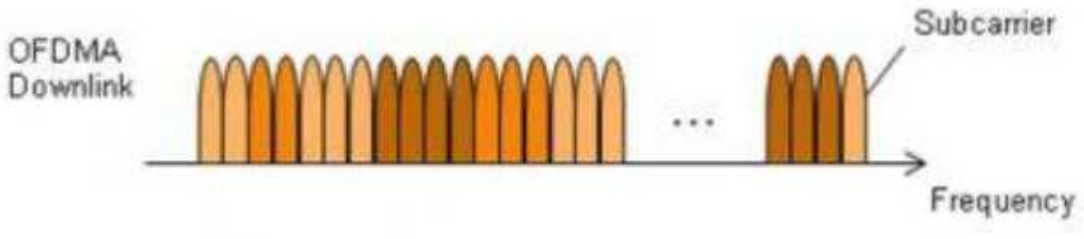

Figure 2.2.4: OFDMA Downlink

Uplink:

LTE uses a pre-coded version of OFDM called Single Carrier Frequency Division Multiple Access (SC-FDMA) in the uplink. This is to compensate for a drawback with normal OFDM, which has a very high Peak to Average Power Ratio (PAPR). High PAPR requires expensive and inefficient power amplifiers with high requirements on linearity, which increases the cost of the terminal and drains the battery faster.

With the RF power amplifier that transmits the radio frequency signal via the antenna to the base station being the highest power item within the mobile, it is necessary that it operates in as efficient mode as possible. This can be significantly affected by the form of radio frequency modulation and signal format. Signals that have a high peak to average ratio and require linear amplification do not lend themselves to the use of efficient RF power amplifiers. As a result it is necessary to employ a mode of transmission that has as near a constant power level when operating. While this is not a problem for the base station where power is not a particular problem, it is unacceptable for the mobile. As a result, LTE uses a modulation scheme known as SC-FDMA - Single Carrier Frequency Division Multiplex which is a hybrid format in the uplink. This combines the low peak to average ratio offered by single-carrier systems with the multipath interference resilience and flexible subcarrier frequency allocation that OFDM provides. A low PAPR also improves coverage and the cell-edge performance.

Figure 2.2.5 shows the Basic SC-FDMA transmission:

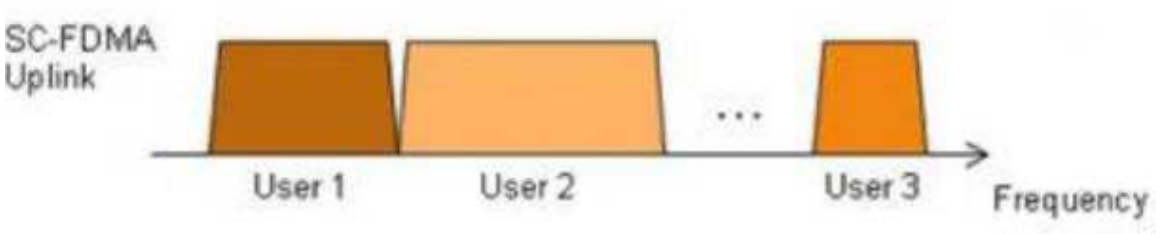

Figure 2.2.5: SC-FDMA Uplink

CHAPTER 3

CHANNEL-SHORTENING METHOD

3.1 Introduction

This method is used when the delay spread of the channel is greater than cyclic prefix duration which results in IOSI , IBI.

In this method, we would be passing the received symbols through a space-time equalizer. This is ,in general, the first stage of the receiver through which symbols pass. The following gives the stage-by-stage process through which symbols pass in receiver side:

- Space-time equalizer
- S/P Conversion
- Cyclic Prefix Removal
- FFT
- Frequency Domain Equalization

In the space-time equalizer, the received symbols will be convolved with a FIR filter whose coefficients are determined based on the channel through which it was transmitted. The number of space-time equalizer blocks to be employed depends on the number of active transmit antennas and the number of equalizers within each block depends on the number of receive antennas. The coefficients are designed in such a way that when

convolved with received symbols, the significant portion of the new channel response will be within cyclic prefix duration thus avoiding IOSI, IBI. This method can also be used when there is interference either coming from another base station or from another antenna of same base station. Then the space-time equalizer coefficients are chosen in such a way that it not only highlights the significant portion of the new channel response but also reduces the effect of the interference term thus eliminating CAI, CCI (**[1]**).

3.2 Mathematical model

Let us consider a scenario of LTE Downlink case. Consider a MIMO System where there are 2 base stations and one receiver (see Figure3.2.1).

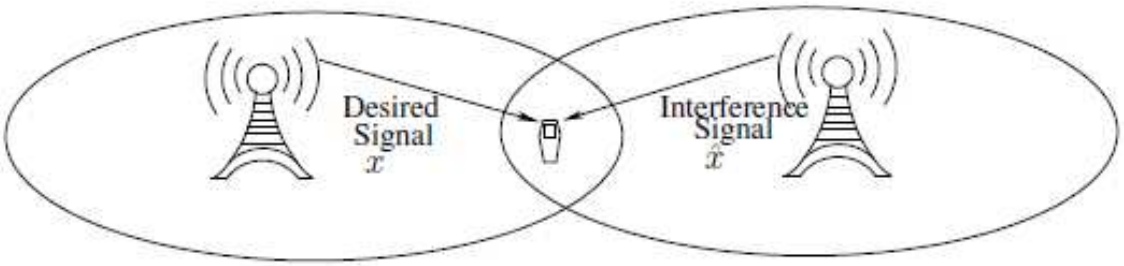

Figure 3.2.1: Interference model adapted from **[2]**

Let M_t be the total number of active transmit antennas (corresponding to 2 base stations)

M be the number of antennas at the desired base station (Base station1)

M_r be the total number of active receive antennas at the receiver

ϑ be the sampled channel impulse response order

L be the order of each filter of space-time equalizer

L_{CP} be the cyclic prefix samples

N be the number of subcarriers

Consider a $M_r \times M_t$ MIMO-OFDM system

$$\overrightarrow{r_j} = \sum_{i=1}^{M_t} (\overrightarrow{h_{ji}} \star \overrightarrow{S_i}) + \overrightarrow{\eta_j} \tag{3.2.1}$$

where j runs from 1 to M_r

$\star$ denotes convolution operator

$\overrightarrow{h_{ji}}$ is the channel vector between i^{th} transmit antenna and j^{th} receiver antenna

$$\overrightarrow{h_{ji}} = \left[h_{ji}(0)\, h_{ji}(1)\, h_{ji}(2) \cdots\cdots\cdots\cdots h_{ji}(\vartheta)\right]^T$$

$\overrightarrow{S_i}$ is the transmitted OFDM symbol from i^{th} transmit antenna

$$\overrightarrow{S_i} = [s_i(N-L_{CP})\, s_i(N-L_{CP}+1) \cdots\cdots s_i(N-1)\, s_i(0)\, s_i(1) \cdots\cdots\cdots s_i(N-1)]^T$$

$\overrightarrow{r_j}$ is the received OFDM symbol at j^{th} receive antenna

$\overrightarrow{\eta_j}$ is the AWGN noise vector at j^{th} receive antenna

Now eq.(3.2.1) can be written as

$$r_j(k) = \sum_{i=1}^{M_t} \sum_{n=0}^{\vartheta} h_{ji}(n) \cdot s_i(k-n) + \eta_j(k) \tag{3.2.2}$$

The received symbol at each antenna is passed through the space-time equalizer and the outputs of the space-time equalizer are added.

As here there are M_t transmit antennas(transmitted symbols), hence there must be M_t space-time equalizers and each equalizer must have M_r filters each of order L.

After passing through the space-time equalizer, we get

$$\overrightarrow{y_i} = \sum_{j=1}^{M_r} (\overrightarrow{w_{ij}} \star \overrightarrow{r_j})$$

where i' runs from 1 to M

$\overrightarrow{w_{i'j}}$ is the filter at j^{th} receive antenna for detecting symbol from i'^{th} transmit antenna.

$$\overrightarrow{w_{i'j}} = \left[w_{i'j}(0)\, w_{i'j}(1)\, w_{i'j}(2) \cdots\cdots\cdots\cdots\cdots w_{i'j}(L) \right]^T$$

$\overrightarrow{y_{i'}}$ is the output of space-time equalizer corresponding to i'^{th} transmit antenna

Now,

$$\begin{aligned} y_{i'}(k) &= \sum_{j=1}^{M_r} \sum_{m=0}^{L} w_{i'j}(m) \cdot r_j(k-m) \qquad (3.2.3) \\ &= \sum_{j=1}^{M_r} \sum_{m=0}^{L} w_{i'j}(m) \cdot \left(\sum_{i=1}^{M_t} \sum_{n=0}^{\vartheta} h_{ji}(n) \cdot s_i(k-(m+n)) + \eta_j(k-m) \right) \end{aligned}$$

This can be written in simpler terms as

$$\overrightarrow{y_{i'}} = \sum_{i=1}^{M_t} \sum_{j=1}^{M_r} (\overrightarrow{w_{i'j}} \star \overrightarrow{h_{ji}}) \star \overrightarrow{S_i} + \underbrace{\sum_{j=1}^{M_r} (\overrightarrow{w_{i'j}} \star \overrightarrow{\eta_j})}_{(\textbf{Colored noise})} \qquad (3.2.4)$$

Now the new target channel impulse response would be

$$\sum_{j=1}^{M_r} (\overrightarrow{w_{i'j}} \star \overrightarrow{h_{ji}})$$

3.3 Channel-Estimate based Equalizer Design

The approach for designing space-time equalizer is to estimate the channel first and then design the equalizer using estimated channel.

3.3.1 Channel Estimation

Here, non-blind channel estimation technique is used. We used block-type pilot arrangement (see Figure 3.3.1) i.e OFDM symbols with pilots at all subcarriers, referred to as pilot symbols are transmitted periodically for channel estimation. This arrangement works well for frequency selective channels as each pilot symbol contains known pilot signals at all of the sub-carriers. However this is suitable only for slow fading channels.

To estimate the channel, all the training sequences of the active antennas in the system have to be known to the receiver.

Here we stack all the training sequences as $S = [S_1\, S_2 \cdots\cdots\cdots S_{M_t}]$

where

$$S_i = \begin{bmatrix} s_i(0) & 0 & \cdots & \cdots & \cdots & \cdots & 0 \\ s_i(1) & s_i(0) & & & & & \vdots \\ \vdots & s_i(1) & \ddots & & & & \vdots \\ \vdots & \vdots & & \ddots & & & \vdots \\ s_i(N-1) & \vdots & & & \ddots & & \vdots \\ 0 & s_i(N-1) & & & & \ddots & \vdots \\ \vdots & 0 & & & & & \vdots \\ \vdots & \vdots & & & & & 0 \\ 0 & 0 & \cdots & \cdots & \cdots & \cdots & s_i(0) \end{bmatrix}$$

Matrix representation is

$$R = SH + N$$

MMSE channel estimate can be obtained as

$$\hat{H} = (S^H S + \sigma_n^2 . I)^{-1} S^H R$$

where σ_n^2 is the noise power

I is the identity matrix

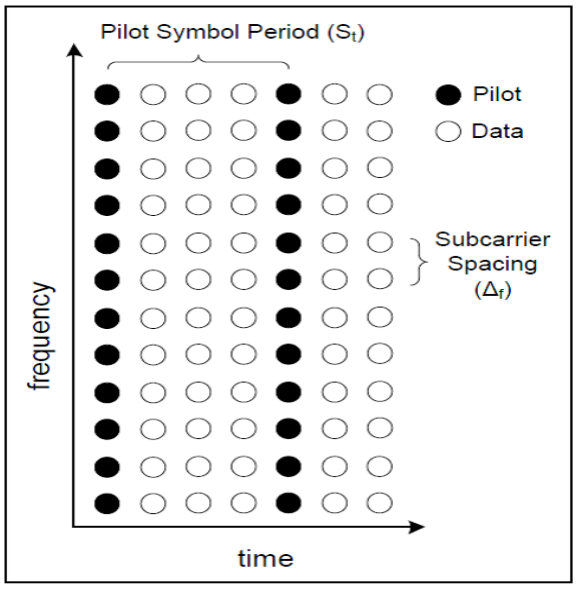

Figure 3.3.1: Block-Type Pilot Arrangement adapted from **[9]**

3.3.2 Objective function to determine space-time equalizer co-efficients

The method used to determine the equalizer co-efficients is Maximum Shortened Signal-to-Interference-and-Noise-Ratio (MSSINR) method. In this, the energy of the components (within cyclic prefix duration) of the target channel impulse response are maximised and the other components are minimized thus eliminating IOSI, IBI, CCI, CAI. Thus the objective function is given as (**[1]**)

$$\max_{w_{i'},\Gamma_i} \frac{w_{i'}^H \hat{H}^H \Gamma_i^H \Gamma_i \hat{H} w_{i'}^H}{w_{i'}^H \hat{H}^H \bar{\Gamma}_i^H \bar{\Gamma}_i \hat{H} w_{i'}^H + \sigma_n^2 I} \qquad s.t \qquad \|w_{i'}\|^2 = 1$$

where Γ_i is the binary diagonal matrix which selects the samples in a certain window of length L_{CP} of the effective target channel response after space-time filtering for i'^{th} transmit antenna.

The matrix $\bar{\Gamma}_i$ selects the samples outside the window. Thus by performing the optimization over $w_{i'}$ and Γ_i, the energy of the post-equalization channel response will be mainly concentrated in the selected window of length L_{CP}, and the energy outside the selected window is minimized.

3.3.3 Matrix Representation

Matrix Representation of eq.(3.2.4) (neglecting noise term) is

$$\mathbf{Y_{i'}} = \mathbf{S} \cdot \mathbf{H} \cdot \mathbf{W_{i'}}$$

where

$$\mathbf{S} = \left[\mathbf{S_1} \vdots \mathbf{S_2} \vdots \cdots\cdots\cdots \vdots \mathbf{S_{M_t}}\right]_{(\mathbf{N}+\mathbf{L_{CP}})\times\mathbf{M_t}(\mathbf{L}+\nu+\mathbf{1})}$$

$$\mathbf{S_i} = \begin{bmatrix} s_i(N-L_{CP}) & 0 & \cdots & \cdots & \cdots & 0 \\ s_i(N-L_{CP}+1) & s_i(N-L_{CP}) & 0 & \cdots & \cdots & 0 \\ \vdots & s_i(N-L_{CP}+1) & & & & \vdots \\ s_i(N-1) & \vdots & \ddots & & & \vdots \\ s_i(0) & s_i(N-1) & & \ddots & & \\ \vdots & s_i(0) & & & \ddots & \\ \vdots & \vdots & & & & \ddots \\ s_i(N-1) & s_i(N-2) & \cdots & \cdots & & \end{bmatrix}_{(\mathbf{N}+\mathbf{L_{CP}})\times(\mathbf{L}+\nu+\mathbf{1})}$$

$$\mathbf{H} = \begin{bmatrix} H_{11} & H_{21} & \cdots & \cdots & H_{M_r 1} \\ H_{12} & H_{22} & \cdots & \cdots & H_{M_r 2} \\ \vdots & \vdots & \vdots & \vdots & \vdots \\ \vdots & \vdots & \vdots & \vdots & \vdots \\ H_{1M_t} & H_{2M_t} & \cdots & \cdots & H_{M_r M_t} \end{bmatrix}_{\mathbf{M_t}(\mathbf{L}+\nu+\mathbf{1})\times\mathbf{M_r}(\mathbf{L}+\mathbf{1})}$$

$$\mathbf{H_{ji}} = \begin{bmatrix} h_{ji}(0) & 0 & \cdots & \cdots & \cdots & 0 \\ h_{ji}(1) & h_{ji}(0) & 0 & \cdots & \cdots & 0 \\ \vdots & h_{ji}(1) & h_{ji}(0) & & & \vdots \\ \vdots & \vdots & \ddots & & & h_{ji}(0) \\ h_{ji}(\nu) & \vdots & & \ddots & & h_{ji}(1) \\ 0 & h_{ji}(\nu) & & & \ddots & \vdots \\ \vdots & 0 & & & & \vdots \\ \vdots & \vdots & & & & \vdots \\ 0 & 0 & \cdots & \cdots & \cdots & h_{ji}(\nu) \end{bmatrix}_{(\mathbf{L}+\vartheta+\mathbf{1})\times(\mathbf{L}+\mathbf{1})}$$

$$\mathbf{W_{i'}} = \begin{bmatrix} W_{i'1} \\ W_{i'2} \\ \vdots \\ \vdots \\ W_{i'M_r} \end{bmatrix}_{\mathbf{M_r}(\mathbf{L}+\mathbf{1})\times\mathbf{1}} \qquad \mathbf{W_{i'j}} = \begin{bmatrix} w_{i'j}(0) \\ w_{i'j}(1) \\ \vdots \\ \vdots \\ \vdots \\ w_{i'j}(L) \end{bmatrix}_{(\mathbf{L}+\mathbf{1})\times\mathbf{1}}$$

Now a window which can take only L_{CP} rows of the matrix $\mathbf{H}$ is chosen such that energy present within the window is maximum and the energy outside the window is minimum.

Let $\mathbf{H_{L_{CP}}}$ be the matrix which contains the significant L_{CP} rows of the matrix $\mathbf{H}$ and $\mathbf{H_{int}}$ be the matrix containing remaining rows of $\mathbf{H}$.

Now

$$\mathbf{H} = \begin{bmatrix} H_{L_{CP}} \\ \cdots\cdots\cdots \\ H_{int} \end{bmatrix}$$

Size of $\mathbf{H_{L_{CP}}}$ is $\mathbf{L_{CP}} \times \mathbf{M_r}(\mathbf{L}+\mathbf{1})$

Size of $\mathbf{H_{int}}$ is $(\mathbf{M_t}(\mathbf{L}+\nu+\mathbf{1}) - \mathbf{L_{CP}}) \times \mathbf{M_r}(\mathbf{L}+\mathbf{1})$

Now to cancel IOSI, IBI, CCI, CAI we need

$$\mathbf{H_{int}} \cdot \mathbf{W_{i'}} = \mathbf{0} \qquad (\textbf{Interference Cancellation condition})$$

Thus $\mathbf{W_{i'}}$ is a non-zero vector which must belong to the null space of matrix $\mathbf{H_{int}}$

$$\Rightarrow dim(null(H_{int})) > 0$$

According to rank-nullity theorem,

$$dim(col(H_{int})) + dim(null(H_{int})) = total\,number\,of\,columns\,of\,H_{int} \tag{3.3.1}$$

As all the elements of H_{int} are independent to each other, hence

$$dim(col(H_{int})) = rank(H_{int}) = M_t(L+\nu+1) - L_{CP}$$

Substituting in eq.(3.3.1), we get

$$(\mathbf{M_t}(\mathbf{L}+\nu+\mathbf{1}) - \mathbf{L_{CP}}) + \mathbf{dim}(\mathbf{null}(\mathbf{H_{int}})) = \mathbf{M_r}(\mathbf{L}+\mathbf{1})$$

$$\Rightarrow \mathbf{dim}(\mathbf{null}(\mathbf{H_{int}})) = \mathbf{M_r}(\mathbf{L}+\mathbf{1}) - (\mathbf{M_t}(\mathbf{L}+\nu+\mathbf{1}) - \mathbf{L_{CP}}) > \mathbf{0}$$

$$\Rightarrow \boxed{L > \frac{M_t(\vartheta+1) - L_{CP} - M_r}{M_r - M_t}} \tag{3.3.2}$$

Thus to use channel-shortening method, we need

$$\boxed{M_r > M_t} \tag{3.3.3}$$

3.4 Frequency Offset Compensation

3.4.1 Introduction

OFDM systems are highly sensitive to the frequency offset. The frequency offset would cause a loss in the orthogonality of the subcarriers thus leading to Inter Carrier Interference (ICI) (see Figure 3.4.1).

Let B be the total channel bandwidth and N be the number of subcarriers then subcarrier bandwidth is $\frac{B}{N}$

∇f be the frequency offset then normalised frequency offset is given as $\xi = \frac{\nabla f}{\left(\frac{B}{N}\right)}$

If P is the transmitted power and σ_n^2 is the noise power then SNR expression due to the frequency offset changes from (**[8]**)

$$\frac{P \mid H \mid^2}{\sigma_n^2} \rightarrow \frac{P \mid H \mid^2 \left(\frac{\sin(\pi\xi)}{\pi\xi}\right)^2}{0.822P \mid H \mid^2 (\sin(\pi\xi))^2 + \sigma_n^2}$$

3.4.2 Mathematical model

Here we assume that frequency offset exists between the local oscillators of the base station and a receiver.

Now eq.(3.2.2) changes to

$$r_j(k) = \sum_{i=1}^{M_t} \sum_{n=0}^{\vartheta} h_{ji}(n) \cdot s_i(k-n) \cdot \exp(j2\pi \frac{\xi_b}{N} k) + \eta_j(k) \qquad , b = 1,2$$

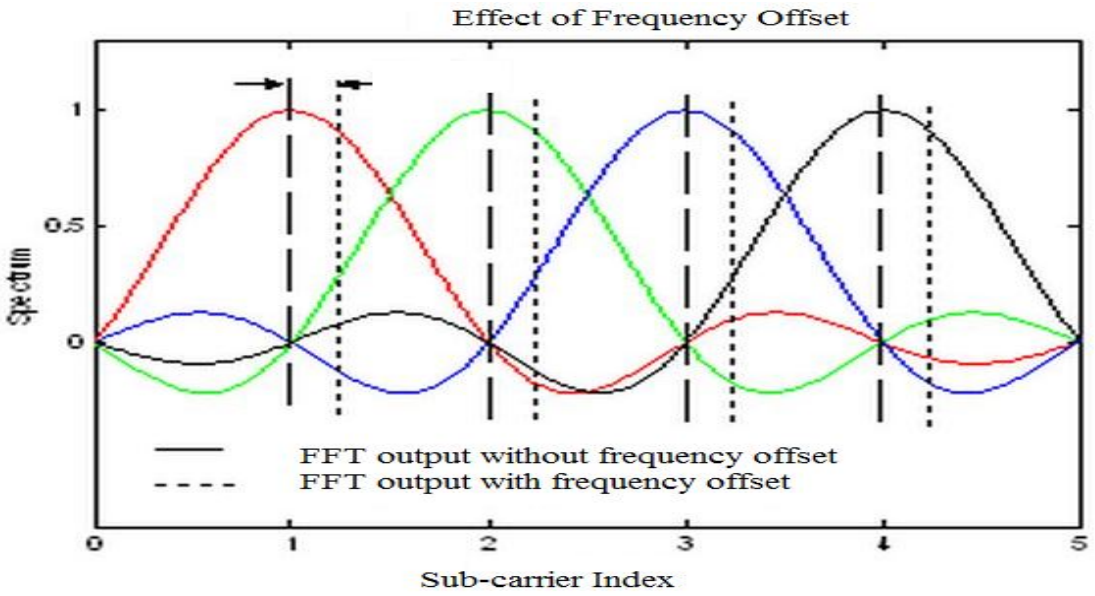

Figure 3.4.1: ICI due to Carrier frequency offset

Hence to compensate frequency offset (assuming base station 1 is desired base station), eq.(3.2.3) changes to (**[3]**)

$$\begin{aligned} y_{i'}(k) &= \sum_{j=1}^{M_r}\sum_{m=0}^{L} w_{i'j}(m)\cdot r_j(k-m)\cdot\exp(-j2\pi\frac{\xi_1}{N}k) \\ &= \sum_{j=1}^{M_r}\sum_{m=0}^{L} w_{i'j}(m)\cdot\left(\sum_{i=1}^{M_t}\sum_{n=0}^{\vartheta} h_{ji}(n)\cdot s_i(k-(m+n))\cdot\exp(j2\pi\frac{\xi_b}{N}(k-m))\right)\cdot\exp(-j2\pi\frac{\xi_1}{N}k) \\ &+ \sum_{j=1}^{M_r}\sum_{m=0}^{L} w_{i'j}(m)\cdot\eta_j(k-m)\cdot\exp(-j2\pi\frac{\xi_1}{N}k) \end{aligned}$$

This gets simplified to

$$\begin{aligned} y_{i'}(k) &= \sum_{j=1}^{M_r}\left(\sum_{x=1}^{M}\sum_{t=0}^{\nu}\left(\sum_{m=0}^{L} w_{i'j}(m)\cdot\exp(-j2\pi\frac{\xi_1}{N}m)\cdot h_{jx}(t-m)\right)\cdot\underbrace{s_x(k-t)}_{(\textbf{desired signal})}\right. \\ &\left.+\sum_{x=M+1}^{M_t}\sum_{t=0}^{\nu}\left(\sum_{m=0}^{L} w_{i'j}(m)\cdot\exp(-j2\pi\frac{\xi_2}{N}m)\cdot h_{jx}(t-m)\right)\cdot\underbrace{s_x(k-t)\cdot\exp(j2\pi\frac{(\xi_2-\xi_1)}{N}k)}_{(\textbf{interference signal})}\right) \\ &+\underbrace{\sum_{j=1}^{M_r}\sum_{m=0}^{L} w_{i'j}(m)\cdot\eta_j(k-m)\cdot\exp(-j2\pi\frac{\xi_1}{N}k)}_{(\textbf{Colored noise})} \end{aligned}$$

Thus the target channel response is given as

$$\sum_{i=1}^{M_t}\sum_{j=1}^{M_r}(\overrightarrow{w^a_{i'j}}\star\overrightarrow{h_{ji}})$$

where

$$w^a_{i'j}(k)=\begin{cases} w_{i'j}(k)\cdot\exp(-j2\pi\frac{\xi_1}{N}k) & \forall i=1\,to\,M \\ w_{i'j}(k)\cdot\exp(-j2\pi\frac{\xi_2}{N}k) & \forall i=M+1\,to\,M_t \end{cases}$$

3.4.3 Matrix Representation

The matrix representation of the new target channel impulse reponse would be

$$\mathbf{H}\cdot\mathbf{W_{i'}}$$

where

$$\mathbf{H} = \begin{bmatrix} \mathbf{H_{11}}.\in_{\mathbf{1}} & \mathbf{H_{21}}.\in_{\mathbf{1}} & \cdots & \cdots & \mathbf{H_{M_r1}}.\in_{\mathbf{1}} \\ \mathbf{H_{12}}.\in_{\mathbf{1}} & \mathbf{H_{22}}.\in_{\mathbf{1}} & \cdots & \cdots & \mathbf{H_{M_r2}}.\in_{\mathbf{1}} \\ \vdots & \vdots & \vdots & \vdots & \vdots \\ \mathbf{H_{1M}}.\in_{\mathbf{1}} & \mathbf{H_{2M}}.\in_{\mathbf{1}} & \cdots & \cdots & \mathbf{H_{M_rM}}.\in_{\mathbf{1}} \\ \mathbf{H_{1(M+1)}}.\in_{\mathbf{2}} & \mathbf{H_{2(M+1)}}.\in_{\mathbf{2}} & \cdots & \cdots & \mathbf{H_{M_r(M+1)}}.\in_{\mathbf{2}} \\ \vdots & \vdots & \vdots & \vdots & \vdots \\ \mathbf{H_{1M_t}}.\in_{\mathbf{2}} & \mathbf{H_{2M_t}}.\in_{\mathbf{2}} & \cdots & \cdots & \mathbf{H_{M_rM_t}}.\in_{\mathbf{2}} \end{bmatrix}_{\mathbf{M_t(L+\nu+1)\times M_r(L+1)}}$$

$$\mathbf{H_{ji}} = \begin{bmatrix} h_{ji}(0) & 0 & \cdots & \cdots & \cdots & 0 \\ h_{ji}(1) & h_{ji}(0) & 0 & \cdots & \cdots & 0 \\ \vdots & h_{ji}(1) & h_{ji}(0) & & & \vdots \\ \vdots & \vdots & \ddots & & & h_{ji}(0) \\ h_{ji}(\nu) & \vdots & & \ddots & & h_{ji}(1) \\ 0 & h_{ji}(\nu) & & & \ddots & \vdots \\ \vdots & 0 & & & & \vdots \\ \vdots & \vdots & & & & \vdots \\ 0 & 0 & \cdots & \cdots & \cdots & h_{ji}(\nu) \end{bmatrix}_{(\mathbf{L}+\vartheta+\mathbf{1})\times(\mathbf{L}+\mathbf{1})}$$

$$\in_{\mathbf{1}} = \begin{bmatrix} 1 & 0 & \cdots & \cdots & 0 \\ 0 & \exp(-j2\pi\frac{\xi_1}{N}.1) & & & \vdots \\ \vdots & & \ddots & & \vdots \\ \vdots & & & \ddots & \vdots \\ 0 & \cdots & \cdots & \cdots & \exp(-j2\pi\frac{\xi_1}{N}.L) \end{bmatrix}_{(\mathbf{L}+\mathbf{1})\times(\mathbf{L}+\mathbf{1})}$$

$$\in_2 = \begin{bmatrix} 1 & 0 & \cdots & \cdots & 0 \\ 0 & \exp(-j2\pi\frac{\xi_2}{N}.1) & & & \vdots \\ \vdots & & \ddots & & \vdots \\ \vdots & & & \ddots & \vdots \\ 0 & \cdots & \cdots & \cdots & \exp(-j2\pi\frac{\xi_2}{N}.L) \end{bmatrix}_{(\mathbf{L}+\mathbf{1})\times(\mathbf{L}+\mathbf{1})}$$

$$\mathbf{W_{i'}} = \begin{bmatrix} W_{i'1} \\ W_{i'2} \\ \vdots \\ \vdots \\ W_{i'M_r} \end{bmatrix}_{\mathbf{M_r}(\mathbf{L}+\mathbf{1})\times\mathbf{1}} \qquad \mathbf{W_{i'j}} = \begin{bmatrix} w_{i'j}(0) \\ w_{i'j}(1) \\ \vdots \\ \vdots \\ \vdots \\ w_{i'j}(L) \end{bmatrix}_{(\mathbf{L}+\mathbf{1})\times\mathbf{1}}$$

Now if we proceed in the same way as it was discussed in sec(3.3.3), we get

$$\boxed{\mathbf{L} > \frac{\mathbf{M_t}(\vartheta + \mathbf{1}) - \mathbf{L_{CP}} - \mathbf{M_r}}{\mathbf{M_r} - \mathbf{M_t}}}$$

Thus to compensate the frequency offset along with the removal of IOSI, IBI, CCI, CAI, we need to choose

$$\boxed{\mathbf{M_r} > \mathbf{M_t}} \tag{3.4.1}$$

Comparing eq.(3.3.3) and eq.(3.4.1), one can conclude that Channel-shortening method can be used to eliminate IOSI, IBI, CCI, CAI, ICI (due to frequency offset) only if the total number of active receive antennas $(M_r)$are chosen to be greater than total number of active transmit antennas (M_t).

Table 3.4.1 gives the conditions for using Channel-Shortening method for different cases of frequency offsets.

Frequency Offsets	**Condition**
$\xi_1 = \xi_2 = 0$	$M_r > M_t$
$\xi_1 = \xi_2 \neq 0$	$M_r > M_t$
$\xi_1 \neq \xi_2 \neq 0$	$M_r > M_t$

Table 3.4.1: Conditions to use Channel-Shortening method for different frequency offsets

CHAPTER 4

PROPOSED METHOD

4.1 Introduction

The Proposed method employs widely-linear filtering alongside to Channel-Shortening method. This additional concept provides an add-on advantage of diversity when compared to Channel-Shortening alone.

To understand the proposed method, let us first discuss the concept of widely-linear filtering.

4.2 Widely-Linear Filtering

Widely-Linear filtering is a new signal processing concept that is being widely used for linear estimation of the signal and its complex conjugate. When the channel response is complex, collecting the complex and complex-conjugate copies of the received signal (alternately collecting the real and imaginary parts), creates two different copies of the signal (See Figure 4.2.1). It was showed that the filtering of these two copies provides an advantage only when the pseudo-covariance (defined as covariance between received signal and its complex conjugate) is non-zero. Such processes with non-zero pseudo-covariance are classified as improper (or) non-circular random processes (**[6]**).

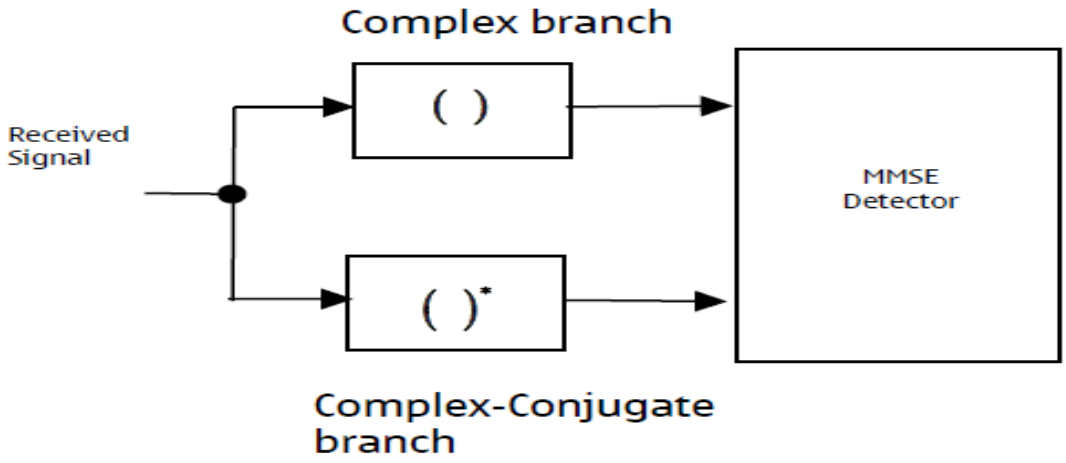

Figure 4.2.1: Widely-Linear filtering adapted from **[6]**

Let y be a scalar random variable and x be a random vector, then

In linear estimation

$$y = h^H x \tag{4.2.1}$$

where h is a complex filter

H denotes conjugate transpose

In Widely Linear filtering,

$$y^{'} = h^H x + g^H x^{\star} \tag{4.2.2}$$

where g is a complex filter

$x^{\star}$ denotes complex-conjugate of x

In eq.(4.2.1), y is a linear function of x, whereas in eq.(4.2.2), $y^{'}$ is not a linear function of x. However the moment of order of $y^{'}$ is completely defined from the moments of order of x and $x^{\star}$, which characterizes a form of linearity. Hence eq.(4.2.2) is called as a wide-sense linear filter (**[7]**).

If the signal is assumed to be circular in nature, then the second term of eq.(4.2.2) disappears in such a way that complex signals can be treated as if they were real. Hence

this WL filtering concept appears to show advantages when the signals are non-circular in nature(pseudo-covariance is non zero). However, there are some situations where the concept proved to work good even for circular signals.

4.3 Proposed Method

The Proposed Method is a combination of Channel-Shortening method and widely linear filtering concept.

$$\textbf{Proposed Method} = \textbf{Channel Shortening Method} + \textbf{Widely Linear Filtering}$$

Using Widely-Linear filtering concept, this method provides a better advantage compared to channel-shortening method.
An illustration is provided for better understanding.

4.3.1 Illustration

Consider a 2x1 (2 receive antennas and 1 transmit antenna) MIMO System.

Let $\vec{x}$ be the transmitted symbol from transmit antenna1
$\overrightarrow{r_1}$ be the received symbol at receive antenna1
$\overrightarrow{r_2}$ be the received symbol at receive antenna2
$\overrightarrow{h_{11}}$ be the channel between transmit antenna1 and receive antenna1
$\overrightarrow{h_{21}}$ be the channel between transmit antenna1 and receive antenna2

Now

$$\begin{aligned} \overrightarrow{r_1} &= \overrightarrow{h_{11}} \star \overrightarrow{x} + \overrightarrow{\eta_1} \\ \overrightarrow{r_2} &= \overrightarrow{h_{21}} \star \overrightarrow{x} + \overrightarrow{\eta_2} \end{aligned}$$

where $\star$ denotes convolution operator

$\overrightarrow{\eta_1}$ is the AWGN noise at receive antenna1

$\overrightarrow{\eta_2}$ is the AWGN noise at receive antenna2

After passing through space-time equalizer, we get

$$\begin{aligned} \overrightarrow{y_1} &= \overrightarrow{w_{11}} \star \overrightarrow{r_1} + \overrightarrow{w_{12}} \star \overrightarrow{r_2} \\ &= \left(\overrightarrow{w_{11}} \star \overrightarrow{h_{11}} + \overrightarrow{w_{12}} \star \overrightarrow{h_{21}}\right) \star \overrightarrow{x} + \left(\overrightarrow{w_{11}} \star \overrightarrow{\eta_1} + \overrightarrow{w_{12}} \star \overrightarrow{\eta_2}\right) \end{aligned} \tag{4.3.1}$$

Consider a 1x1 (1 receive antenna and 1 transmit antenna) MIMO System.

Let $\vec{x}$ be the transmitted symbol from transmit antenna1

$\overrightarrow{r_1}$ be the received symbol at receive antenna1

$\overrightarrow{h_{11}}$ be the channel between transmit antenna1 and receive antenna1

Now

$$\overrightarrow{r_1} = \overrightarrow{h_{11}} \star \overrightarrow{x} + \overrightarrow{\eta_1}$$

After passing through space-time equalizer which uses the widely-linear filtering concept, we get

$$\overrightarrow{y_1} = \overrightarrow{w_{11}} \star \overrightarrow{r_1} + \overrightarrow{w_{12}} \star \overrightarrow{r_1^\star}$$

where $\overrightarrow{r_1^\star}$ denotes the omplex conjugate of $\overrightarrow{r_1}$

$$\Longrightarrow \overrightarrow{y_1} = \left(\overrightarrow{w_{11}} \star \overrightarrow{h_{11}}\right) \star \overrightarrow{x} + \left(\overrightarrow{w_{12}} \star \overrightarrow{h_{11}^\star}\right) \star \overrightarrow{x^\star} + \left(\overrightarrow{w_{11}} \star \overrightarrow{\eta_1} + \overrightarrow{w_{12}} \star \overrightarrow{\eta_1^\star}\right)$$

If $\overrightarrow{x} = \overrightarrow{x^\star}$,the

$$\Longrightarrow \overrightarrow{y_1} = \left(\overrightarrow{w_{11}} \star \overrightarrow{h_{11}} + \overrightarrow{w_{12}} \star \overrightarrow{h_{11}^\star}\right) \star \overrightarrow{x} + + \left(\overrightarrow{w_{11}} \star \overrightarrow{\eta_1} + \overrightarrow{w_{12}} \star \overrightarrow{\eta_1^\star}\right) \tag{4.3.2}$$

Comparing eqs.(4.3.1) and (4.3.2), one can conclude that a 1x1 system using widely-linear filtering concept can be made to act like a 2x1 system using traditional linear filtering if $\overrightarrow{x} = \overrightarrow{x^\star}$ i.e the transmitted symbols must be real.

To make transmitted symbols real $\left(\overrightarrow{x} = \overrightarrow{x^{\star}}\right)$

In the transmitter side, we first do subcarrier mapping of the symbols onto the subcarriers and then take IFFT of all the subcarriers.

The IFFT equation is given as

$$\begin{aligned} x(u) &= \frac{1}{N}\sum_{i=0}^{N-1} a_i \exp(j\frac{2\pi}{N}\cdot i\cdot u) \\ &= \frac{1}{N}\left(a_0 + a_1\exp(j\frac{2\pi}{N}\cdot 1\cdot u) + \cdots\cdots\cdots + a_{N-1}\exp(j\frac{2\pi}{N}\cdot(N-1)\cdot u)\right) \end{aligned} \tag{4.3.3}$$

This can also be written as

$$x(u) = \frac{1}{N}\left(a_0 + a_1\exp(-j\frac{2\pi}{N}\cdot(N-1)\cdot u) + \cdots\cdots\cdots + a_{N-1}\exp(-j\frac{2\pi}{N}\cdot 1\cdot u)\right) \tag{4.3.4}$$

Taking conjugate of eq.(4.3.3), we get

$$x^{\star}(u) = \frac{1}{N}\left(a_0^{\star} + a_1^{\star}\exp(-j\frac{2\pi}{N}\cdot 1\cdot u) + \cdots\cdots\cdots + a_{N-1}^{\star}\exp(-j\frac{2\pi}{N}\cdot(N-1)\cdot u)\right) \tag{4.3.5}$$

Comparing eqs. (4.3.4) and (4.3.5), one can conclude that $x(u) = x^{\star}(u)$ if

$$\begin{aligned} a_0 &= a_0^{\star} \\ a_{\frac{N}{2}} &= a_{\frac{N}{2}}^{\star} \\ a_m &= a_n^{\star} \, where \, m+n = N \end{aligned}$$

Subcarrier mapping

Let us assume that there are N subcarriers ($\frac{-N}{2}$ to $\frac{N}{2}-1$) out of which there are M data subcarriers. Take $\frac{M}{2}$ symbols (a_i) and map them on the subcarriers ranging from $\left(\frac{-M}{2}\right)$ to (-1) and map the conjugate of these symbols in the reverse order from $(1)$to $\left(\frac{M}{2}\right)$ such that data on the m^{th} sub-carrier is equal to conjugate of the data on n^{th} sub-carrier where $m+n=0$ is satisfied. This kind of subcarrier mapping makes the transmitted

symbols real (see Figure 4.3.1). But bit rate gets reduced to half (as only half the subcarriers carry useful data) compared to Channel-Shortening method.

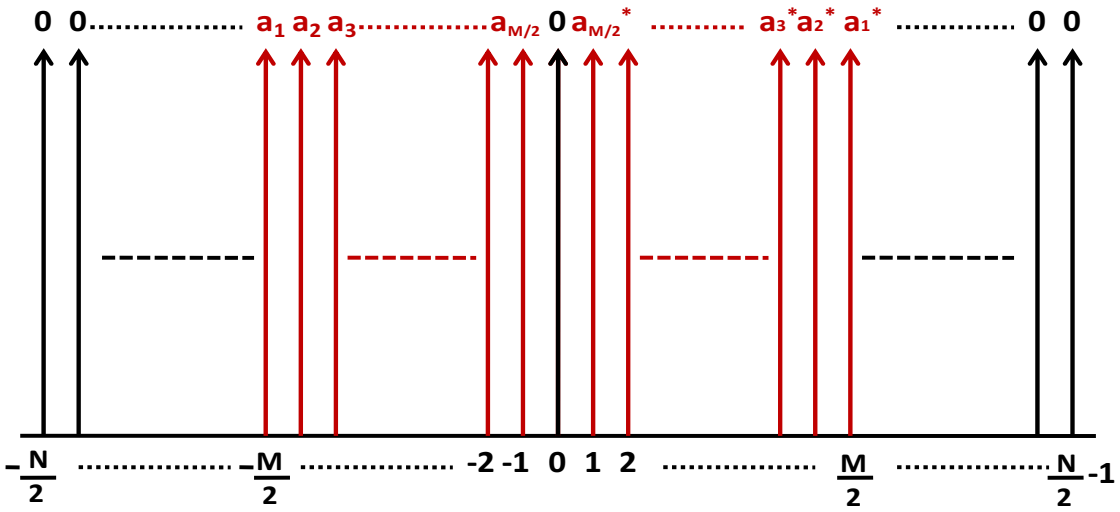

Figure 4.3.1: Sub-carrier mapping

4.3.2 Mathematical model

Consider a MIMO System where there are 2 base stations and one receiver (See Figure 4.3.2).

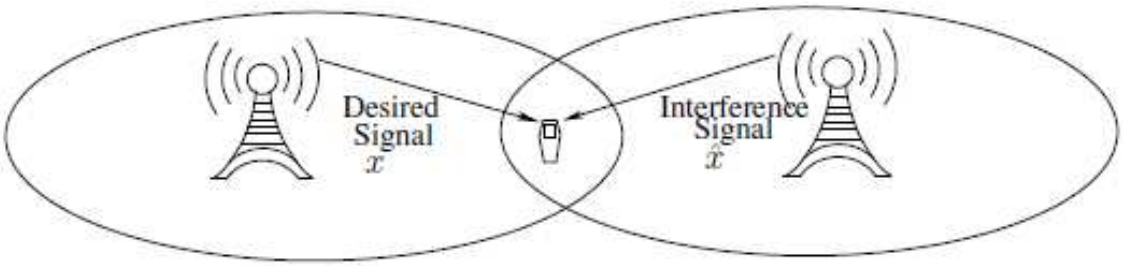

Figure 4.3.2: Interference model adapted from **[2]**

Let M_t be the total number of active transmit antennas(corresponding to 2 base stations)

M be the number of antennas at the desired base station (Base station1)

M_r be the total number of active receive antennas at the receiver

ϑ be the sampled channel impulse response order

L be the order of each filter of space-time equalizer

L_{CP} be the cyclic prefix samples

N be the number of subcarriers

Consider a $M_r \times M_t$ MIMO-OFDM system

$$\overrightarrow{r_j} = \sum_{i=1}^{M_t} (\overrightarrow{h_{ji}} \star \overrightarrow{S_i}) + \overrightarrow{\eta_j} \tag{4.3.6}$$

where j runs from 1 to M_r

$\star$ denotes convolution operator

$\overrightarrow{h_{ji}}$ is the channel vector between i^{th}transmit antenna and j^{th}receiver antenna

$$\overrightarrow{h_{ji}} = \left[h_{ji}(0)\, h_{ji}(1)\, h_{ji}(2) \cdots\cdots\cdots\cdots\cdots h_{ji}(\vartheta)\right]^T$$

$\overrightarrow{S_i}$ is the transmitted OFDM symbol from i^{th}transmit antenna

$$\overrightarrow{S_i} = [s_i(N-L_{CP})\, s_i(N-L_{CP}+1) \cdots\cdots s_i(N-1)\, s_i(0)\, s_i(1) \cdots\cdots\cdots s_i(N-1)]^T$$

$\overrightarrow{r_j}$ is the received OFDM symbol at j^{th}receive antenna

$\overrightarrow{\eta_j}$ is the AWGN noise vector at j^{th}receive antenna

Now eq.(4.3.6) can be written as

$$r_j(k) = \sum_{i=1}^{M_t} \sum_{n=0}^{\vartheta} h_{ji}(n) \cdot s_i(k-n) + \eta_j(k) \tag{4.3.7}$$

The received symbol at each antenna is passed through the space-time equalizer which use widely-linear filtering and the outputs of the space-time equalizer are added.

As here there are M_t transmit antennas(transmitted symbols), hence there must be M_t space-time equalizers and each equalizer must have M_r filters each of order L.

After passing through the space-time equalizer, we get

$$\overrightarrow{y_{i'}} = \sum_{j=1}^{M_r} (\overrightarrow{w_{i'j}} \star \overrightarrow{r_j}) + \sum_{j=1}^{M_r} (\overrightarrow{w^{'}_{i'j}} \star \overrightarrow{r_j^{\star}})$$

where i' runs from 1 to M

$\overrightarrow{w_{i'j}}$ and $\overrightarrow{w^{'}_{i'j}}$ are the filter at j^{th} receive antenna for detecting symbol from i'^{th} transmit antenna

$$\begin{aligned} \overrightarrow{w_{i'j}} &= \left[w_{i'j}(0)\, w_{i'j}(1)\, w_{i'j}(2) \cdots\cdots\cdots\cdots\cdots w_{i'j}(L) \right]^T \\ \overrightarrow{w^{'}_{i'j}} &= \left[w^{'}_{i'j}(0)\, w^{'}_{i'j}(1)\, w^{'}_{i'j}(2) \cdots\cdots\cdots\cdots\cdots w^{'}_{i'j}(L) \right]^T \end{aligned}$$

$\overrightarrow{y_{i'}}$ is the output of space-time equalizer corresponding to i'^{th} transmit antenna

Now,

$$\begin{aligned} y_{i'}(k) &= \sum_{j=1}^{M_r} \sum_{m=0}^{L} w_{i'j}(m) \cdot r_j(k-m) + \sum_{j=1}^{M_r} \sum_{m=0}^{L} w^{'}_{i'j}(m) \cdot r_j^{\star}(k-m) \qquad (4.3.8) \\ &= \sum_{j=1}^{M_r} \sum_{m=0}^{L} w_{i'j}(m) \cdot \left(\sum_{i=1}^{M_t} \sum_{n=0}^{\vartheta} h_{ji}(n) \cdot s_i(k-(m+n)) + \eta_j(k-m) \right) \\ &+ \sum_{j=1}^{M_r} \sum_{m=0}^{L} w^{'}_{i'j}(m) \cdot \left(\sum_{i=1}^{M_t} \sum_{n=0}^{\vartheta} h^{\star}_{ji}(n) \cdot s^{\star}_i(k-(m+n)) + \eta^{\star}_j(k-m) \right) \end{aligned}$$

This can be written in simpler terms as

$$\overrightarrow{y_{i'}} = \sum_{i=1}^{M_t} \sum_{j=1}^{M_r} \left((\overrightarrow{w_{i'j}} \star \overrightarrow{h_{ji}}) \star \overrightarrow{S_i} + (\overrightarrow{w^{'}_{i'j}} \star \overrightarrow{h^{\star}_{ji}}) \star \overrightarrow{S^{\star}_i} \right) + \sum_{j=1}^{M_r} \left(\overrightarrow{w_{i'j}} \star \overrightarrow{\eta_j} + \overrightarrow{w^{'}_{i'j}} \star \overrightarrow{\eta^{\star}_j} \right)$$

Since $\overrightarrow{S_i} = \overrightarrow{S^{\star}_i}$, we get

$$\overrightarrow{y_i} = \sum_{i=1}^{M_t} \sum_{j=1}^{M_r} \left((\overrightarrow{w_{i'j}} \star \overrightarrow{h_{ji}} + \overrightarrow{w^{'}_{i'j}} \star \overrightarrow{h^{\star}_{ji}}) \star \overrightarrow{S_i} \right) + \underbrace{\sum_{j=1}^{M_r} \left(\overrightarrow{w_{i'j}} \star \overrightarrow{\eta_j} + \overrightarrow{w^{'}_{i'j}} \star \overrightarrow{\eta^{\star}_j} \right)}_{(\textbf{Colored noise})} \qquad (4.3.9)$$

Now the new target channel impulse response would be

$$\sum_{i=1}^{M_t}\sum_{j=1}^{M_r}(\overrightarrow{w_{i'j}}\star\overrightarrow{h_{ji}}+\overrightarrow{w^{\downarrow}_{i'j}}\star\overrightarrow{h^{\star}_{ji}}) \tag{4.3.10}$$

The same channel estimation scheme (sec.3.3.1) and the same objective function (sec.3.3.2) are used here to determine channel taps and space-time equalizer coefficients resp.

4.3.3 Matrix Representation

Matrix Representation of eq.(3.2.4) (neglecting noise term) is

$$\mathbf{Y_{i'}} = \mathbf{S}\cdot\mathbf{H}\cdot\mathbf{W_{i'}}$$

where

$$\mathbf{S} = \Big[\mathbf{S_1}\vdots\mathbf{S_2}\vdots\cdots\cdots\vdots\mathbf{S_{M_t}}\Big]_{(\mathbf{N}+\mathbf{L_{CP}})\times\mathbf{M_t}(\mathbf{L}+\nu+\mathbf{1})}$$

$$\mathbf{S_i} = \begin{bmatrix} s_i(N-L_{CP}) & 0 & \cdots & \cdots & \cdots & 0 \\ s_i(N-L_{CP}+1) & s_i(N-L_{CP}) & 0 & \cdots & \cdots & 0 \\ \vdots & s_i(N-L_{CP}+1) & & & & \vdots \\ s_i(N-1) & \vdots & \ddots & & & \vdots \\ s_i(0) & s_i(N-1) & & \ddots & & \\ \vdots & s_i(0) & & & \ddots & \\ \vdots & \vdots & & & & \ddots \\ s_i(N-1) & s_i(N-2) & \cdots & \cdots & & \end{bmatrix}_{(\mathbf{N}+\mathbf{L_{CP}})\times(\mathbf{L}+\nu+\mathbf{1})}$$

$$\mathbf{H} = \begin{bmatrix} H_{11} & H_{11}^{\star} & H_{21} & H_{21}^{\star} & \cdots & \cdots & H_{M_r 1} & H_{M_r 1}^{\star} \\ H_{12} & H_{12}^{\star} & H_{22} & H_{22}^{\star} & \cdots & \cdots & H_{M_r 2} & H_{M_r 2}^{\star} \\ \vdots & \vdots & \vdots & \vdots & \vdots & \vdots & \vdots & \vdots \\ \vdots & \vdots & \vdots & \vdots & \vdots & \vdots & \vdots & \vdots \\ H_{1M_t} & H_{1M}^{\star} & H_{2M_t} & H_{2M_t}^{\star} & \cdots & \cdots & H_{M_r M_t} & H_{M_r M_t}^{\star} \end{bmatrix}_{\mathbf{M_t(L+\nu+1)\times 2M_r(L+1)}}$$

$$\mathbf{H_{ji}} = \begin{bmatrix} h_{ji}(0) & 0 & \cdots & \cdots & \cdots & 0 \\ h_{ji}(1) & h_{ji}(0) & 0 & \cdots & \cdots & 0 \\ \vdots & h_{ji}(1) & h_{ji}(0) & & & \vdots \\ \vdots & \vdots & \ddots & & & h_{ji}(0) \\ h_{ji}(\nu) & \vdots & & \ddots & & h_{ji}(1) \\ 0 & h_{ji}(\nu) & & & \ddots & \vdots \\ \vdots & 0 & & & & \vdots \\ \vdots & \vdots & & & & \vdots \\ 0 & 0 & \cdots & \cdots & \cdots & h_{ji}(\nu) \end{bmatrix}_{\mathbf{(L+\vartheta+1)\times(L+1)}}$$

$$\mathbf{W_{i'}} = \begin{bmatrix} W_{i'1} \\ W_{i'1}^{'} \\ W_{i'2} \\ W_{i'2}^{'} \\ \vdots \\ \vdots \\ W_{i'M_r} \\ W_{i'M_r}^{'} \end{bmatrix}_{\mathbf{2M_r(L+1)\times 1}} \qquad \mathbf{W_{i'j}} = \begin{bmatrix} w_{i'j}(0) \\ w_{i'j}(1) \\ \vdots \\ \vdots \\ \vdots \\ w_{i'j}(L) \end{bmatrix}_{\mathbf{(L+1)\times 1}} \qquad \mathbf{W_{i'j}^{'}} = \begin{bmatrix} w_{i'j}^{'}(0) \\ w_{i'j}^{'}(1) \\ \vdots \\ \vdots \\ \vdots \\ w_{i'j}^{'}(L) \end{bmatrix}_{\mathbf{(L+1)\times 1}}$$

Now a window which can take only L_{CP} rows of the matrix H is chosen such that energy present within the window is maximum and the energy outside the window is minimum. Let $\mathbf{H_{L_{CP}}}$ be the matrix which contains the significant L_{CP} rows of the matrix $\mathbf{H}$ and $\mathbf{H_{int}}$ be the matrix containing remaining rows of $\mathbf{H}$.

Now

$$\mathbf{H} = \begin{bmatrix} H_{L_{CP}} \\ \cdots\cdots\cdots \\ H_{int} \end{bmatrix}$$

Size of $\mathbf{H_{L_{CP}}}$ is $\mathbf{L_{CP} \times 2M_r(L+1)}$

Size of $\mathbf{H_{int}}$ is $\mathbf{(M_t(L+\nu+1) - L_{CP}) \times 2M_r(L+1)}$

Now to cancel IOSI, IBI, CCI, CAI we need

$$\mathbf{H_{int} \cdot W_{i'} = 0} \qquad \mathbf{(Interference\,Cancellation\,condition)}$$

Thus $\mathbf{W_{i'}}$ is a non-zero vector which must belong to the null space of matrix $\mathbf{H_{int}} \Rightarrow$ $dim(null(H_{int})) > 0$

According to rank-nullity theorem,

$$dim(col(H_{int})) + dim(null(H_{int})) = total\,number\,of\,columns\,of\,H_{int} \qquad (4.3.11)$$

As all the elements of H_{int} are independent to each other, hence

$$dim(col(H_{int})) = rank(H_{int}) = M_t(L+\nu+1) - L_{CP}$$

Substituting in eq.(4.3.11), we get

$$\mathbf{(M_t(L+\nu+1) - L_{CP}) + dim(null(H_{int})) = 2M_r(L+1)}$$

$$\Rightarrow \mathbf{dim(null(H_{int})) = 2M_r(L+1) - (M_t(L+\nu+1) - L_{CP}) > 0}$$

$$\Rightarrow \boxed{\mathbf{L > \frac{M_t(\vartheta+1) - L_{CP} - 2M_r}{2M_r - M_t}}} \qquad (4.3.12)$$

Thus to use proposed method, we need

$$\mathbf{2M_r} \quad > \quad \mathbf{M_t}$$

$$\Rightarrow \boxed{\mathbf{M_r} > \frac{\mathbf{M_t}}{\mathbf{2}}} \tag{4.3.13}$$

Thus from eq.(4.3.13), one can conclude that the proposed method can be used to eliminate IOSI, IBI, CCI, CAI if the total number of active receive antennas $(M_r)$are atleast equal to half the number of total active transmit antennas (M_t).

4.4 Frequency Offset Compensation

4.4.1 Mathematical model

OFDM systems are highly sensitive to the frequency offset. The frequency offset would cause a loss in the orthogonality of the subcarriers thus leading to Inter Carrier Interference (ICI).

Let B be the total channel bandwidth and N be the number of subcarriers then subcarrier bandwidth is $\frac{B}{N}$

∇f be the frequency offset then normalised frequency offset is given as $\xi = \frac{\nabla f}{\left(\frac{B}{N}\right)}$

Here we assume that frequency offset exists between the local oscillators of the base station and a receiver.

Now eq.(4.3.7) changes to

$$r_j(k) = \sum_{i=1}^{M_t} \sum_{n=0}^{\vartheta} h_{ji}(n) \cdot s_i(k-n) \cdot \exp(j2\pi \frac{\xi_b}{N} k) + \eta_j(k) \qquad , b = 1,2$$

Hence to compensate frequency offset (assuming base station 1 is desired base station), eq.(4.3.8) changes to

$$
\begin{aligned}
y_{i'}(k) &= \sum_{j=1}^{M_r}\sum_{m=0}^{L} w_{i'j}(m)\cdot r_j(k-m)\cdot\exp(-j2\pi\frac{\xi_1}{N}k) \\
&+ \sum_{j=1}^{M_r}\sum_{m=0}^{L} w^{|}_{i'j}(m)\cdot r_j^{\star}(k-m)\cdot\exp(j2\pi\frac{\xi_1}{N}k) \\
&= \sum_{j=1}^{M_r}\sum_{m=0}^{L} w_{i'j}(m)\cdot\left(\sum_{i=1}^{M_t}\sum_{n=0}^{\vartheta} h_{ji}(n)\cdot s_i(k-(m+n))\cdot\exp(j2\pi\frac{\xi_b}{N}(k-m))\right)\cdot\exp(-j2\pi\frac{\xi_1}{N}k) \\
&+ \sum_{j=1}^{M_r}\sum_{m=0}^{L} w_{i'j}(m)\cdot\eta_j(k-m)\cdot\exp(-j2\pi\frac{\xi_1}{N}k) \\
&+ \sum_{j=1}^{M_r}\sum_{m=0}^{L} w^{|}_{i'j}(m)\cdot\left(\sum_{i=1}^{M_t}\sum_{n=0}^{\vartheta} h_{ji}^{\star}(n)\cdot s_i^{\star}(k-(m+n))\cdot\exp(-j2\pi\frac{\xi_b}{N}(k-m))\right)\cdot\exp(j2\pi\frac{\xi_1}{N}k) \\
&+ \sum_{j=1}^{M_r}\sum_{m=0}^{L} w^{|}_{i'j}(m)\cdot\eta_j^{\star}(k-m)\cdot\exp(j2\pi\frac{\xi_1}{N}k)
\end{aligned}
$$

This gets simplified to

$$
\begin{aligned}
y_{i'}(k) &= \sum_{j=1}^{M_r}\Bigg(\sum_{x=1}^{M}\sum_{t=0}^{\nu}\Bigg(\sum_{m=0}^{L} w_{i'j}(m)\cdot\exp(-j2\pi\frac{\xi_1}{N}m)\cdot h_{jx}(t-m) \\
&+ w^{|}_{i'j}(m)\cdot\exp(j2\pi\frac{\xi_1}{N}m)\cdot h_{jx}^{\star}(t-m)\Bigg)\cdot\underbrace{s_x(k-t)}_{(\textbf{desired signal})} \\
&+ \sum_{x=M+1}^{M_t}\sum_{t=0}^{\nu}\left(\sum_{m=0}^{L} w_{i'j}(m)\cdot\exp(-j2\pi\frac{\xi_2}{N}m)\cdot h_{jx}(t-m)\right)\cdot\underbrace{s_x(k-t)\cdot\exp(j2\pi\frac{(\xi_2-\xi_1)}{N}k)}_{(\textbf{interference signal})} \\
&+ \sum_{x=M+1}^{M_t}\sum_{t=0}^{\nu}\left(\sum_{m=0}^{L} w^{|}_{i'j}(m)\cdot\exp(j2\pi\frac{\xi_2}{N}m)\cdot h_{jx}^{\star}(t-m)\right)\cdot\underbrace{s_x(k-t)\cdot\exp(j2\pi\frac{(\xi_1-\xi_2)}{N}k)}_{(\textbf{interference signal})}\Bigg) \\
&+ \underbrace{\sum_{j=1}^{M_r}\sum_{m=0}^{L} w_{i'j}(m)\cdot\eta_j(k-m)\cdot\exp(-j2\pi\frac{\xi_1}{N}k)+\sum_{j=1}^{M_r}\sum_{m=0}^{L} w^{|}_{i'j}(m)\cdot\eta_j^{\star}(k-m)\cdot\exp(j2\pi\frac{\xi_1}{N}k)}_{(\textbf{Colored noise})}
\end{aligned}
$$

Let $x=\sum_{i=1}^{M_t}\sum_{j=1}^{M_r}(\overrightarrow{w_{i'j}^{a}}\star\overrightarrow{h_{ji}})$ and $y=\sum_{i=1}^{M_t}\sum_{j=1}^{M_r}(\overrightarrow{w_{i'j}^{b}}\star\overrightarrow{h_{ji}})$

where

$$w^{a}_{i'j}(k) = \begin{cases} w_{i'j}(k) \cdot \exp(-j2\pi\frac{\xi_1}{N}k) & \forall i = 1 to M \\ w_{i'j}(k) \cdot \exp(-j2\pi\frac{\xi_2}{N}k) & \forall i = M+1 to M_t \end{cases}$$

$$w^{b}_{i'j}(k) = \begin{cases} w^{|}_{i'j}(k) \cdot \exp(j2\pi\frac{\xi_1}{N}k) & \forall i = 1 to M \\ w^{|}_{i'j}(k) \cdot \exp(j2\pi\frac{\xi_2}{N}k) & \forall i = M+1 to M_t \end{cases}$$

Thus the new target channel response would be

$$\begin{cases} x+y & \forall i = 1 to M \\ x, y & \forall i = M+1 to M_t \end{cases}$$

4.4.2 Matrix Representation

The matrix representation of the new target channel impulse response would be

$$\mathbf{H} \cdot \mathbf{W_{i'}}$$

where

$$\mathbf{H} = \begin{bmatrix} H_{11}.\in_1 & H^{\star}_{11}.\in^{\star}_1 & \cdots & \cdots & H_{M_r1}.\in_1 & H^{\star}_{M_r1}.\in^{\star}_1 \\ H_{12}.\in_1 & H^{\star}_{12}.\in^{\star}_1 & \cdots & \cdots & H_{M_r2}.\in_1 & H^{\star}_{M_r2}.\in^{\star}_1 \\ \vdots & \vdots & \vdots & \vdots & \vdots & \vdots \\ H_{1M}.\in_1 & H^{\star}_{1M}.\in^{\star}_1 & \cdots & \cdots & H^{\star}_{M_rM}.\in_1 & H^{\star}_{M_rM}.\in^{\star}_1 \\ H_{1(M+1)}.\in_2 & 0 & \cdots & \cdots & H_{M_r(M+1)}.\in_2 & 0 \\ 0 & H^{\star}_{1(M+1)}.\in^{\star}_2 & \cdots & \cdots & 0 & H^{\star}_{M_r(M+1)}.\in^{\star}_2 \\ \vdots & \vdots & \vdots & \vdots & \vdots & \vdots \\ H_{1M_t}.\in_2 & 0 & \cdots & \cdots & H_{M_rM_t}.\in_2 & 0 \\ 0 & H^{\star}_{1M_t}.\in^{\star}_2 & \cdots & \cdots & 0 & H^{\star}_{M_rM_t}.\in^{\star}_2 \end{bmatrix}_{(\mathbf{2M_t-M})(\mathbf{L+\nu+1})\times\mathbf{2M_r(L+1}}$$

$$\in_{\mathbf{1}} = \begin{bmatrix} 1 & 0 & \cdots & \cdots & 0 \\ 0 & \exp(-j2\pi\frac{\xi_1}{N}.1) & & & \vdots \\ \vdots & & \ddots & & \vdots \\ \vdots & & & \ddots & \vdots \\ 0 & \cdots & \cdots & \cdots & \exp(-j2\pi\frac{\xi_1}{N}.L) \end{bmatrix}_{(\mathbf{L+1})\times(\mathbf{L+1})}$$

$$\in_{\mathbf{2}} = \begin{bmatrix} 1 & 0 & \cdots & \cdots & 0 \\ 0 & \exp(-j2\pi\frac{\xi_2}{N}.1) & & & \vdots \\ \vdots & & \ddots & & \vdots \\ \vdots & & & \ddots & \vdots \\ 0 & \cdots & \cdots & \cdots & \exp(-j2\pi\frac{\xi_2}{N}.L) \end{bmatrix}_{(\mathbf{L+1})\times(\mathbf{L+1})}$$

$$\mathbf{W_{i'}} = \begin{bmatrix} W_{i'1} \\ W^{|}_{i'1} \\ W_{i'2} \\ W^{|}_{i'2} \\ \vdots \\ \vdots \\ W_{i'M_r} \\ W^{|}_{i'M_r} \end{bmatrix}_{\mathbf{2M_r(L+1)\times 1}} \qquad \mathbf{W_{i'j}} = \begin{bmatrix} w_{i'j}(0) \\ w_{i'j}(1) \\ \vdots \\ \vdots \\ \vdots \\ w_{i'j}(L) \end{bmatrix}_{(\mathbf{L+1})\times\mathbf{1}} \qquad \mathbf{W^{|}_{i'j}} = \begin{bmatrix} w^{|}_{i'j}(0) \\ w^{|}_{i'j}(1) \\ \vdots \\ \vdots \\ \vdots \\ w^{|}_{i'j}(L) \end{bmatrix}_{(\mathbf{L+1})\times\mathbf{1}}$$

Now if we proceed in the same way as it was discussed in sec(4.3.3), we get

$$\boxed{\mathbf{L} > \frac{(\mathbf{2M_t} - \mathbf{M})\cdot(\vartheta + \mathbf{1}) - \mathbf{L_{CP}} - \mathbf{2M_r}}{\mathbf{2M_r} - (\mathbf{2M_t} - \mathbf{M})}} \tag{4.4.1}$$

Thus to compensate the frequency offset along with the removal of IOSI, IBI, CCI, CAI, we need to choose

$$\mathbf{2M_r} > \mathbf{2M_t} - \mathbf{M}$$

$$\Rightarrow \boxed{\mathbf{M_r} > \mathbf{M_t} - \frac{\mathbf{M}}{\mathbf{2}}} \tag{4.4.2}$$

Thus from eq.(4.4.2), the proposed method can be used to eliminate IOSI, IBI, CCI, CAI, ICI(due to frequency offset) only if the total number of active receive antennas $(M_r)$are atleast equal to the total number of active transmit antennas (M_t)minus half the number of total active antennas at the desired base station (M).

If all the antennas belong to the same base station (or) if the local oscillators of the two base stations are synchronized in such a way that $\xi_1 = \xi_2$ then $M = M_t$ and condition changes to $$\mathbf{M_r > \frac{M_t}{2}}$$ which is similar to the case when $\xi_1 = \xi_2 = 0$

Table 4.4.1 gives the conditions for using Proposed method for different cases of frequency offsets.

Frequency Offsets	**Condition**
$\xi_1 = \xi_2 = 0$	$M_r > \frac{M_t}{2}$
$\xi_1 = \xi_2 \neq 0$	$M_r > \frac{M_t}{2}$
$\xi_1 \neq \xi_2 \neq 0$	$M_r > M_t$-$\frac{M}{2}$

Table 4.4.1: Conditions to use proposed method for different frequency offsets

Table 4.4.2 highlights the diversity advantage provided by the Proposed Method compared to the Channel-Shortening method for different cases of frequency offsets.

	Channel-shortening method	**Proposed method**
$\xi_1 = \xi_2 = 0$	$M_r > M_t$	$M_r > \frac{M_t}{2}$
$\xi_1 = \xi_2 \neq 0$	$M_r > M_t$	$M_r > \frac{M_t}{2}$
$\xi_1 \neq \xi_2 \neq 0$	$M_r > M_t$	$M_r > M_t - \frac{M}{2}$

Table 4.4.2: Channel-shortening method vs Proposed method

CHAPTER 5

SIMULATION RESULTS AND DISCUSSION

5.1 Simulation Environment

Table 5.1.1 provides specifications used for various simulation parameters.

Parameter	**Specification**
Channel Bandwidth	5 MHz
Transmission Bandwidth	4.5 MHz
Number of total Subcarriers	512
Number of Data Subcarriers	300
Sub-Carrier Spacing	15 KHz
Sampling Frequency	7.68 MHz
Cyclic Prefix Duration	$4.69\mu s$ (36 samples)
Frequency Domain Equalization	MMSE
Channel RMS Delay Spread	$5.34\mu s$ (41 samples)
MIMO Systems	3×3,4×3
Modulation schemes used	4QAM (Channel-Shortening Method)
	16QAM (Proposed Method)

Table 5.1.1: Simulation Environment

All through the simulations, the channel is assumed to be block-wise time invariant. Here, 2 blocks were transmitted from each antenna where each block will have 24 OFDM symbols+1 training OFDM symbol. The channel is estimated using Least Squares method. No estimation was carried for Frequency offset. BER is calculated by considering 500 independent channel realizations for each SNR.

Also we considered a scenario where 2 base stations are present out of which one is the desired base station and the other is the interference base station. The desired base station is having two transmit antennas and the undesired base station is having 1 transmit antenna (total 3 transmit antennas). Simulations were done taking 3 receive antennas in one case and 4 receive antennas in the other case. For each case, results were shown for zero frequency offsets and also for different frequency offsets (also considering $\frac{C}{I} = 0dB, 6dB$). As the bit rate gets reduced to half in the Proposed method, we used different modulation schemes i.e 4QAM for Channel-Shortening (CS) Method and 16QAM for Proposed method. In this way, same bit rate is maintained in both the methods.

5.2 Simulation Results

Figures 5.2.1-5.2.2 show the performance of a 3×3 MIMO system with both the methods under similar environments.

From these figures, one can understand the diversity improvement provided by the Proposed method compared to Channel-Shortening method.

As $M_r = M_t$, Channel-Shortening method fails whereas Proposed method works if space-time equalizer order is chosen as follows

$$\begin{aligned} L &> \frac{M_t(\nu+1) - L_{CP} - 2M_r}{2M_r - M_t} \\ \Rightarrow L &> 27 \end{aligned}$$

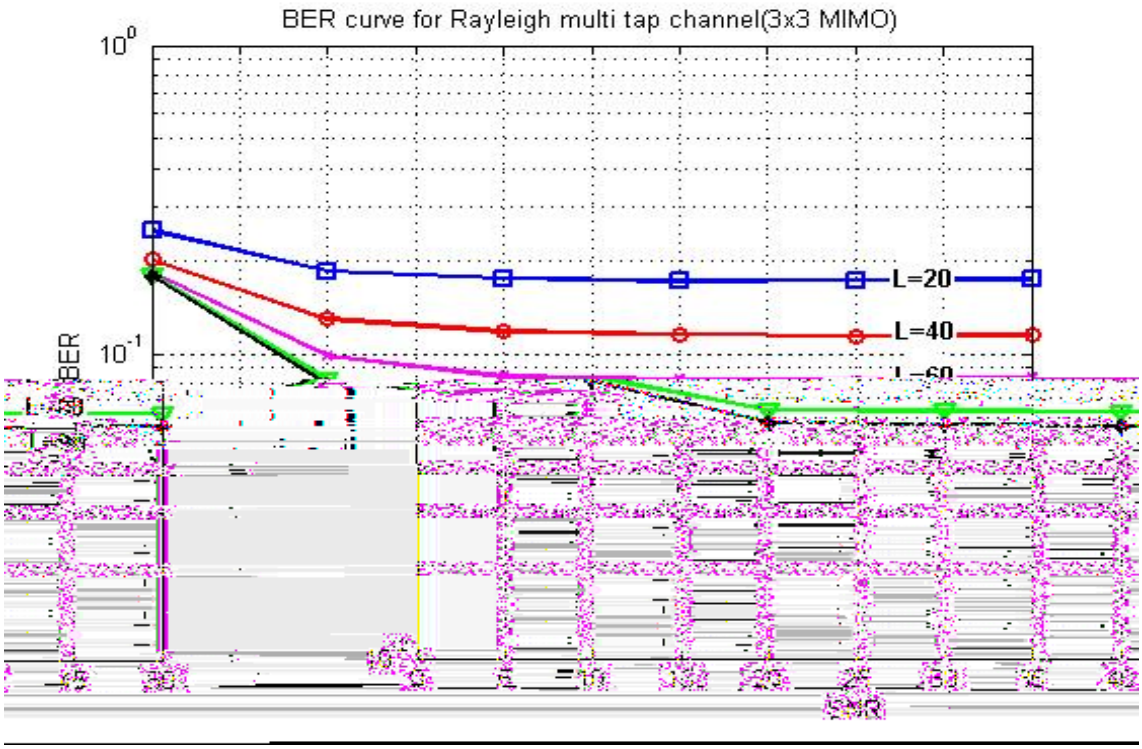

Figure 5.2.1: BER curve for a 3×3 MIMO for different values of equalizer orders for $\frac{C}{I} = 0dB$ and $\xi_1 = \xi_2 = 0$ using Channel-Shortening Method

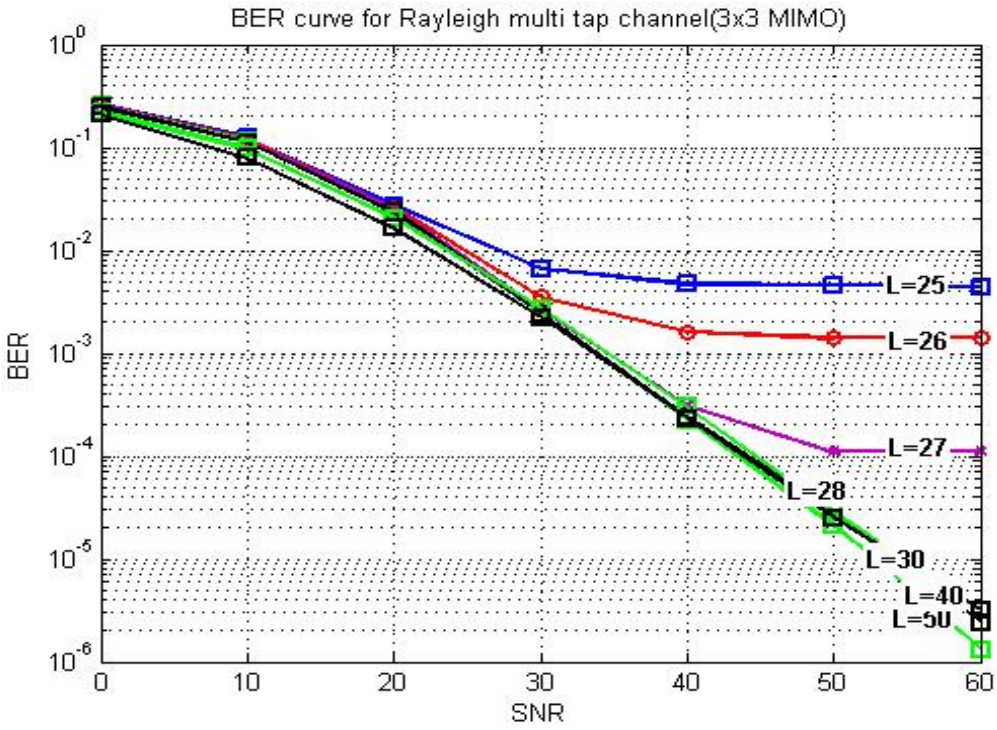

Figure 5.2.2: BER curve for a 3×3 MIMO for different values of equalizer orders for $\frac{C}{I} = 0dB$ and $\xi_1 = \xi_2 = 0$ using Proposed Method

Case (i): $\xi_1 = \xi_2 = 0$

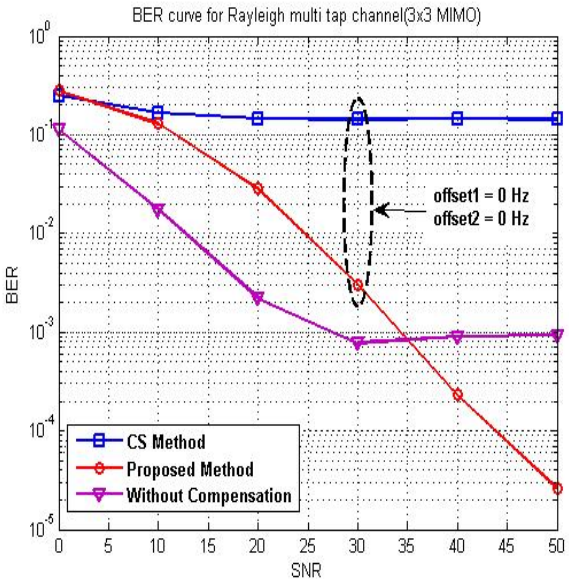

(a) $\frac{C}{I} = 0dB$

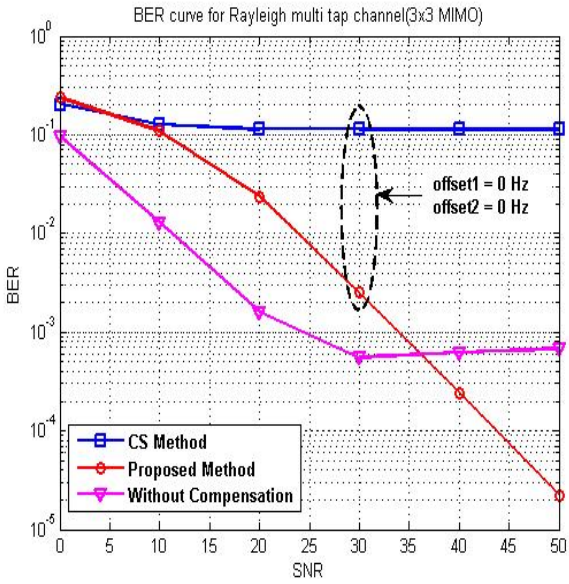

(b) $\frac{C}{I} = 6dB$

Figure 5.2.3: $\mathbf{L = 30, \xi_1 = \xi_2 = 0}$. Figure compares the Performance of a 3×3 MIMO system using both the methods for two cases of $\frac{C}{I} = 0dB$ and $\frac{C}{I} = 6dB$

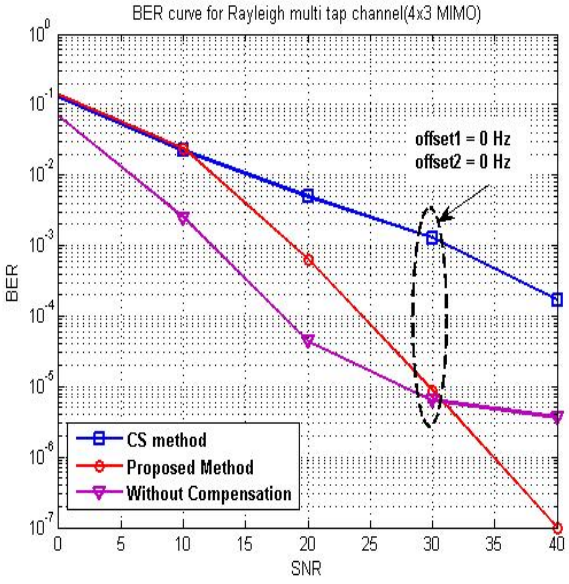

(a) $\frac{C}{I} = 0dB$

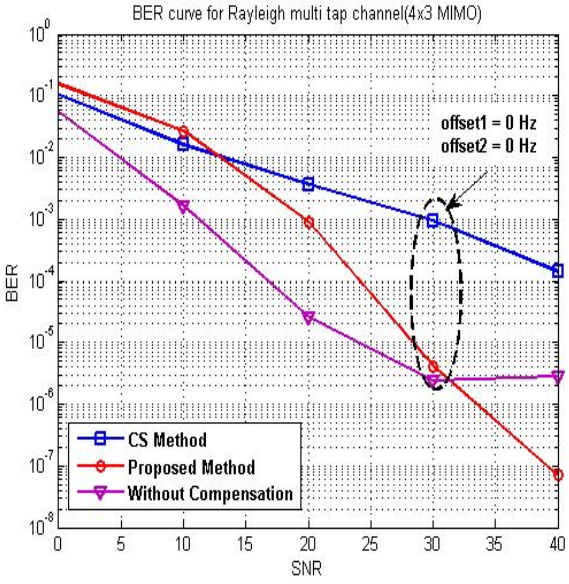

(b) $\frac{C}{I} = 6dB$

Figure 5.2.4: $\mathbf{L = 85, \xi_1 = \xi_2 = 0}$. Figure compares the Performance of a 4×3 MIMO system using both the methods for two cases of $\frac{C}{I} = 0dB$ and $\frac{C}{I} = 6dB$

Case (ii): $\xi_1 = \xi_2 \neq 0$

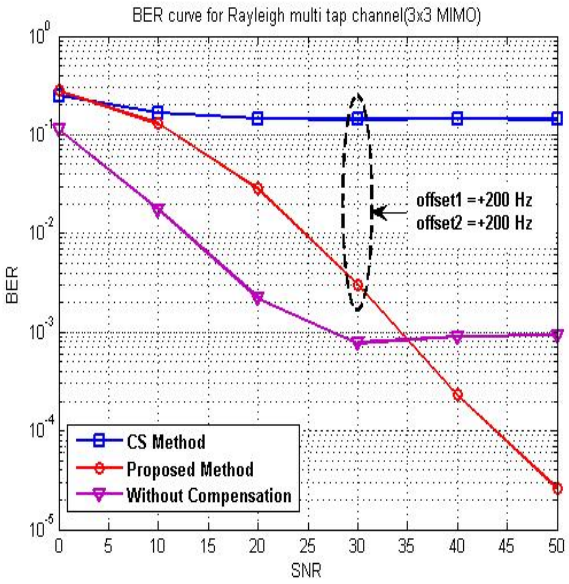

(a) $\frac{C}{I} = 0dB$

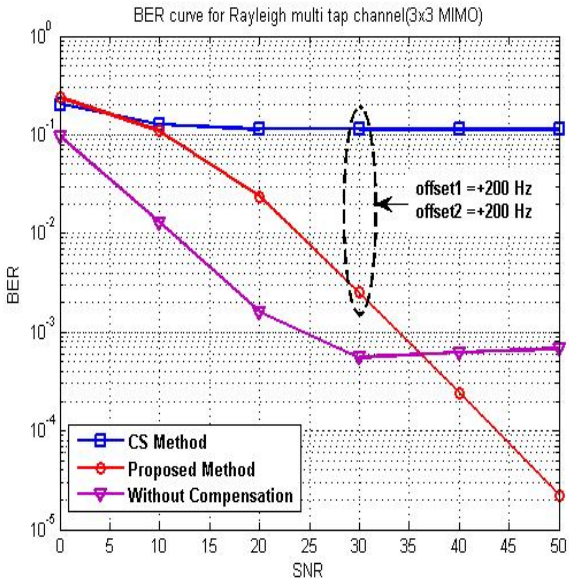

(b) $\frac{C}{I} = 6dB$

Figure 5.2.5: $\mathbf{L = 30, \xi_1 = \xi_2 = 0.0133}$. Figure compares the Performance of a 3×3 MIMO system using both the methods for two cases of $\frac{C}{I} = 0dB$ and $\frac{C}{I} = 6dB$

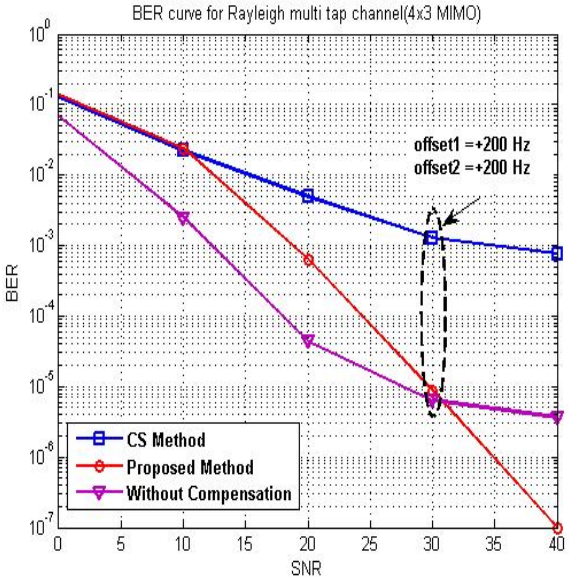

(a) $\frac{C}{I} = 0dB$

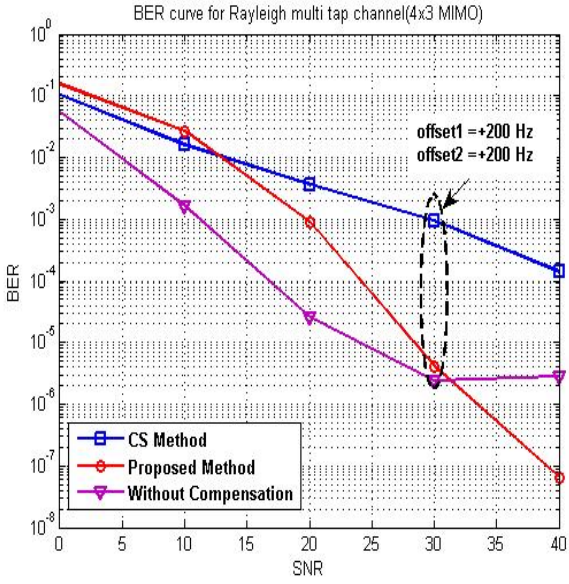

(b) $\frac{C}{I} = 6dB$

Figure 5.2.6: $\mathbf{L = 85, \xi_1 = \xi_2 = 0.0133}$. Figure compares the Performance of a 4×3 MIMO system using both the methods for two cases of $\frac{C}{I} = 0dB$ and $\frac{C}{I} = 6dB$

Case (iii): $\xi_1 \neq \xi_2 \neq 0$

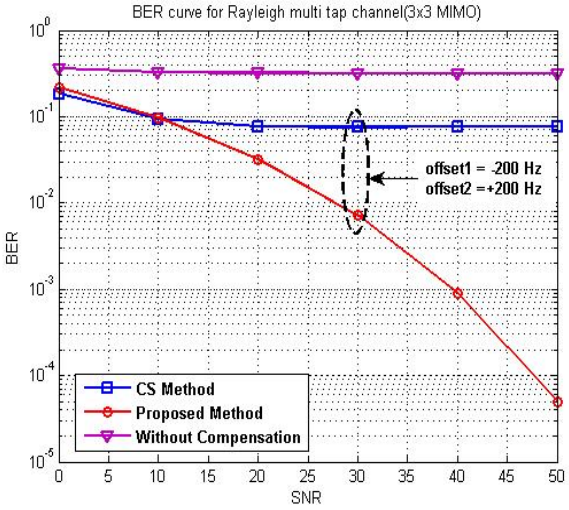

(a) $\frac{C}{I} = 0dB$

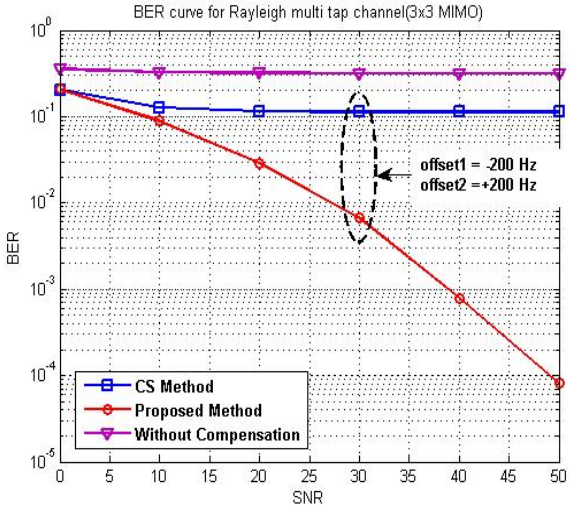

(b) $\frac{C}{I} = 6dB$

Figure 5.2.7: $\mathbf{L = 65, \xi_1 = -0.0133; \xi_2 = 0.0133}$. Figure compares the Performance of a 3×3 MIMO system using both the methods for two cases of $\frac{C}{I} = 0dB$ and $\frac{C}{I} = 6dB$

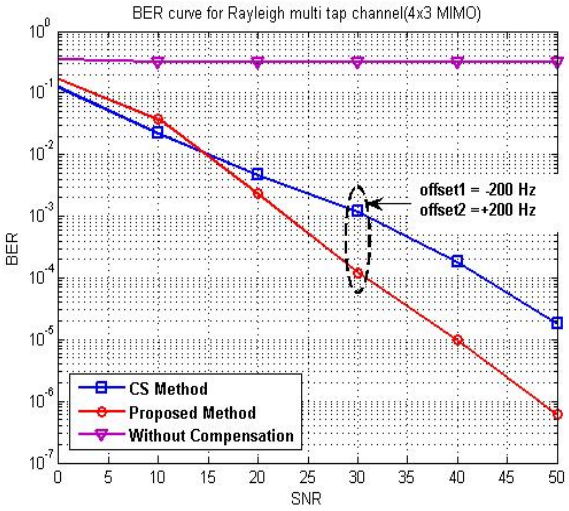

(a) $\frac{C}{I} = 0dB$

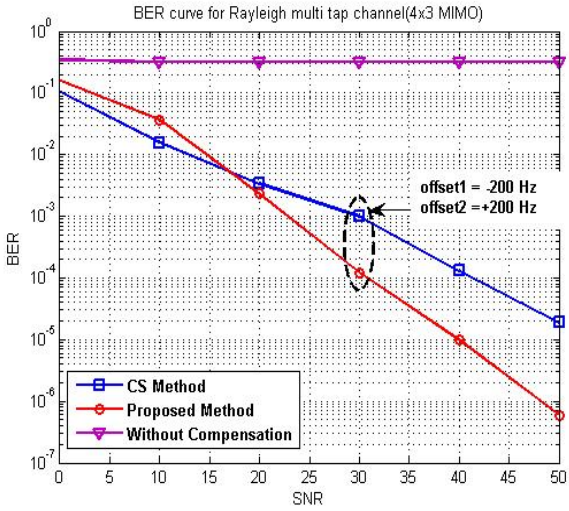

(b) $\frac{C}{I} = 6dB$

Figure 5.2.8: $\mathbf{L = 85, \xi_1 = -0.0133; \xi_2 = 0.0133}$. Figure compares the Performance of a 4×3 MIMO system using both the methods for two cases of $\frac{C}{I} = 0dB$ and $\frac{C}{I} = 6dB$

Figures 5.2.3-5.2.4 compare the performance of the 3×3 and 4×3 MIMO systems using both the methods for different cases of $\frac{C}{I} = 0dB$ and $\frac{C}{I} = 6dB$. One can notice a

slightly higher BER for $\frac{C}{I} = 0dB$ compared to $\frac{C}{I} = 6dB$ because of higher CCI. Also there is no frequency offset between each base station and receiver thus ignoring ICI problem. For this case, the Proposed method is providing a diversity improvement by a factor of 2 compared to CS method thus making the receiver to use lesser number of antennas. Hence when total transmit antennas are 3, CS method requires atleast 4 receive antennas whereas Proposed method requires a minimum of only 2 receive antennas to eliminate the problems caused due to all kinds of interferences.

Figures 5.2.5-5.2.6 compares the performance of the 3×3 and 4×3 MIMO systems using both the methods for non-zero equal frequency offsets thus considering ICI problem too. For this case also, the Proposed method would be providing a diversity improvement by a factor of 2 compared to CS method thus making the receiver to have less number of antennas. For this case, when the total transmit antennas are 3, CS method requires atleast 4 receive antennas whereas Proposed method requires a minimum of only 2 receive antennas to eliminate all interference problems (including ICI).

Figures 5.2.7-5.2.8 compares the performance of the 3×3 and 4×3 MIMO systems using both the methods for non-zero unequal frequency offsets (introduces ICI). In this case, diversity improvement would be provided by Proposed method, but less than 2 and greater than 1, compared to CS method thus making the receiver again to have less number of antennas. Here, when the total transmit antennas are 3, CS method requires atleast 4 receive antennas whereas Proposed method requires a minimum of only 3 receive antennas to eliminate all interference problems (including ICI).

Hence, in simple words

- **For zero frequency offsets, a 3×3 MIMO using Proposed Method is equivalent to 6×3 MIMO using Channel-Shortening method.**
- **For non-zero equal frequency offsets, a 3×3 MIMO using Proposed Method is equivalent to 6×3 MIMO using Channel-Shortening method.**
- **For non-zero unequal frequency offsets, a 3×3 MIMO using Proposed Method is equivalent to 6×4 MIMO using Channel-Shortening method.**

KALMAN FILTER FOR SUN POSITION ESTIMATION

CHAPTER 6

SUN SENSORS AND KALMAN FILTERING ALGORITHM

6.1 Introduction

A normal sized satellite usually weighs more than 500kg, is a few metres long and cost more than 1million Euro to build and launch. However, the smaller satellites: Micro, Nano and Pico (Pico Satellites (see Figure 6.1.1) are about the size of an Hungarian Cube: $10 \times 10 \times 10$ cm and weight less then 1kg) are cheaper to construct and launch, and can do several specific tasks even better than large satellites. Because of their small size, all onboard components are energy thrifty, and their entire surface is used to collect energy from the sun using solar panels.

As of today, there is an increase in the number of Micro, Nano and Pico satellites, launched by many countries from Europe to the United States. These tiny satellites test some breakthrough technologies. This is mainly because the smaller price-to-pay in case of failure. We will also see more satellites flying as a cluster. The reason for that is that a cluster of small satellites is cheaper to construct and maintain and can perform more complex jobs than the single unit.

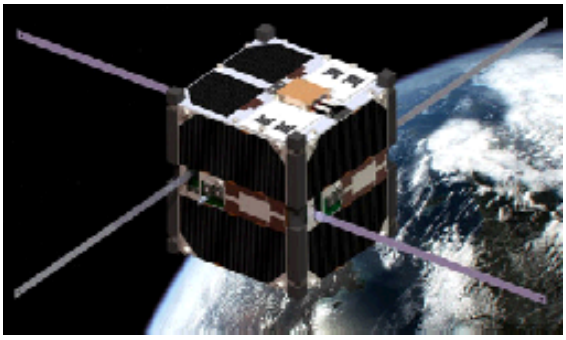

Figure 6.1.1: Image of a Pico Satellite adapted from **[11]**

6.2 Position Sensitive Device

One of the options for a sun sensor is to use a position sensitive device (PSD). A Position Sensitive Device and/or Position Sensitive Detector (PSD) is an optical position sensor (OPS), that can measure a position of a light spot in one or two-dimensions on a sensor surface. A PSD has a single large active area, typically around 1 square centimetre. The PSD works much the same as a typical photodiode. In a photodiode, there is a single PN junction. The diode is reverse-biased and therefore no current flows. When photons of sufficient energy strikes the diode, they excite electrons, causing mobile electrons and holes. This creates a current which is linearly proportional to the illumination of the sensor. A PSD also has a single PN junction. When photons hit the top of the sensor(the p-doped silicon) they cause current to flow. There are four electrodes, two on the x-axis, and two on the y-axis. The current at each of the four electrodes is inversely proportional to the distance from the electrode to the centroid of the light incident upon the sensor. The position of the incident light can be accurately determined using the relative strengths of the currents of each of the four electrodes.

We chose to use a PSD for a number of reasons. Because of the nature of the sensor, no centroiding algorithm is necessary. The analog readings from the sensor are already the centroid of the incident light. This will save computing time on a spacecraft.

6.2.1 Basic Principle

A PSD basically consists of a uniform resistive layer formed on one or both surfaces of a high-resistivity semi-conductor substrate, and a pair of electrodes formed on both ends of the resistive layer for extracting position signals. The active area, which is also a resistive layer, has a PN junction that generates photocurrent by means of the photovoltaic effect.

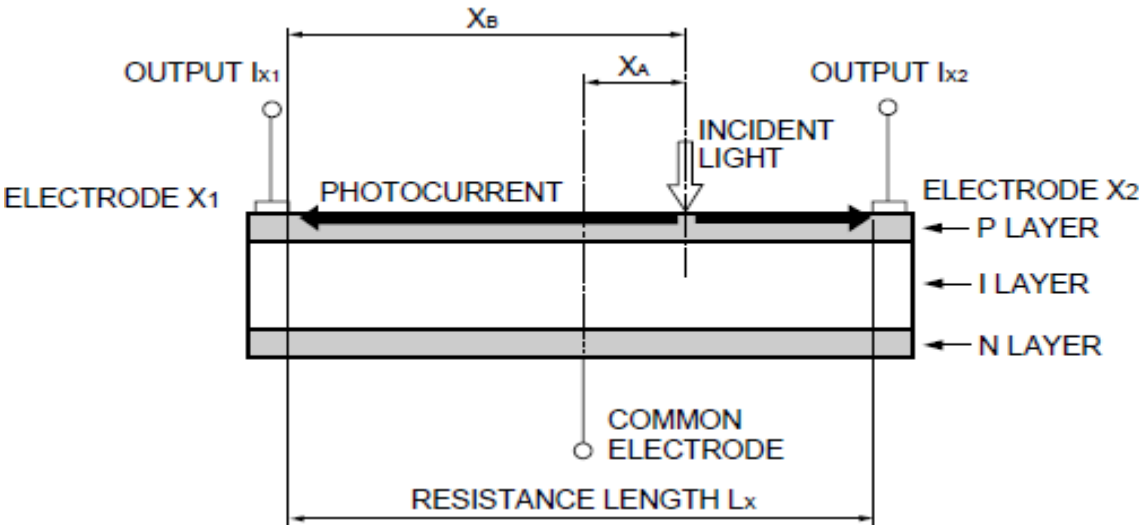

Figure 6.2.1: PSD Sectional view adapted from **[16]**

Figure 6.2.1 shows a sectional view of a PSD using a simple illustration to explain the operating principle. The PSD has a P-type resistive layer formed on an N-type high-resistive silicon substrate. This P-layer serves as an active area for photoelectric conversion and a pair of output electrodes are formed on the both ends of the P-layer. On the backside of the silicon substrate is an N-layer to which a common electrode is connected. Basically, this is the same structure as that of PIN photodiodes except for the P-type resistive layer on the surface.

When a spot light strikes the PSD, an electric charge proportional to the light intensity is generated at the incident position. This electric charge is driven through the resistive layer and collected by the output electrodes X_1 and X_2 as photocurrents, while being

divided in inverse proportion to the distance between the incident position and each electrode.

The relation between the incident light position and the photocurrents from the output electrodes X_1, X_2 is given by the following formulae:

- When the centre point of PSD is set at the origin

$$I_{X_1} = \frac{\frac{L_X}{2} - X_A}{L_X} \times I_0 \quad ; \quad I_{X_2} = \frac{\frac{L_X}{2} + X_A}{L_X} \times I_0$$

$$\Rightarrow \frac{I_{X_2} - I_{X_1}}{I_{X_2} + I_{X_1}} = \frac{2X_A}{L_X} \quad \Rightarrow \frac{I_{X_1}}{I_{X_2}} = \frac{L_X - 2X_A}{L_X + 2X_A}$$

- When the end of the PSD is set at the origin

$$I_{X_1} = \frac{L_X - X_B}{L_X} \times I_0 \quad ; \quad I_{X_2} = \frac{X_B}{L_X} \times I_0$$

$$\Rightarrow \frac{I_{X_2} - I_{X_1}}{I_{X_2} + I_{X_1}} = \frac{2X_B - L_X}{L_X} \quad \Rightarrow \frac{I_{X_1}}{I_{X_2}} = \frac{L_X - X_B}{X_B}$$

where I_0 is the total photocurrent $(I_{X_1} + I_{X_2})$
I_{X_1} is the output current from electrode X_1
I_{X_2} is the output current from electrode X_2
L_X is the resistance length (length of the active area)
X_A is the distance from the electric centre of the PSD to light input position
X_B is the distance from the electrode X_1 of the PSD to light input position

By finding the difference or ratio of I_{X_1} to I_{X_2}, the light input position can be obtained by the formulae irrespective of the incident light intensity level and its changes. The light input position obtained here corresponds to the centre-of-gravity of the light beam.

6.2.2 Types of PSD

The two types of PSD's are:

1. **One-Dimensional PSD**

   Figure 6.2.2 shows the equivalent circuit and structure chart of the One-Dimensional PSD.

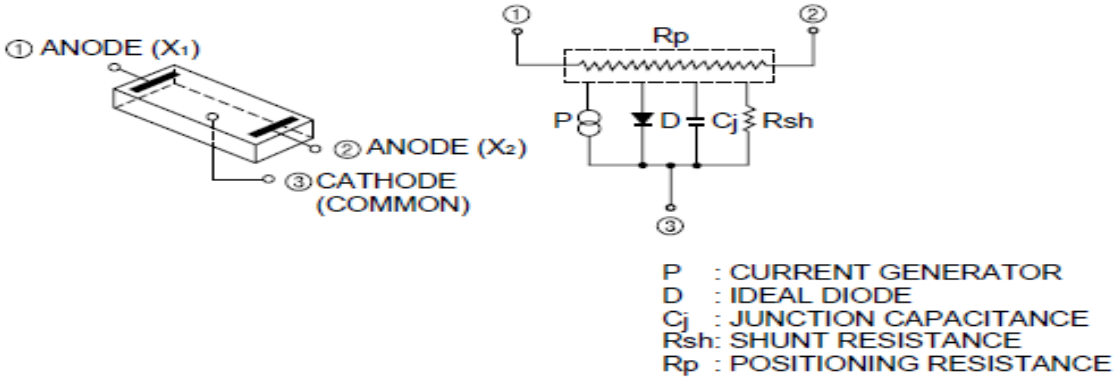

Figure 6.2.2: Structure chart, Equivalent circuit adapted from **[16]**

$$\frac{I_{X_2} - I_{X_1}}{I_{X_2} + I_{X_1}} = \frac{2x}{L_X}$$

In the above formula, I_{X_1} and I_{X_2} are the output currents obtained from the electrodes as shown in Figure 6.2.3.

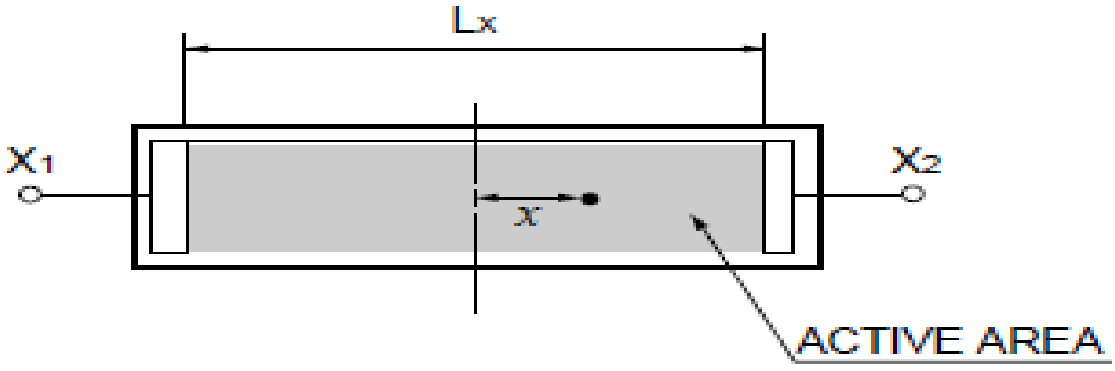

Figure 6.2.3: Active Area Chart adapted from **[16]**

2. **Two-Dimensional PSD**

They are grouped by structure into duo-lateral and tetra-lateral types. Among the tetra-lateral type PSD's, a pin-cushion type with an improved active area and electrodes is also provided. The position conversion formulae slightly differ according to the PSD structure. Two-dimensional PSD's have two pairs of output electrodes X_1, X_2 and Y_1, Y_2.

(a) **Duo-lateral Type PSD**

On the duo-lateral type, the N-layer is processed to form a resistive layer, and two pairs of electrodes are formed on both surfaces as X and Y electrodes are arranged at right angles. The X position signals are extracted from the X electrodes on the upper surface, while the Y position signals are extracted from the Y electrodes on the bottom surface. As shown in Figure 6.2.4, a photocurrent with a polarity opposite that of the other surface is on each surface, to produce signal currents twice as large as the tetra-lateral type and achieve a higher position resolution. In addition, when compared to the tetra-lateral type, the duo-lateral type offers excellent position detection characteristics because the electrodes are not in close proximity.

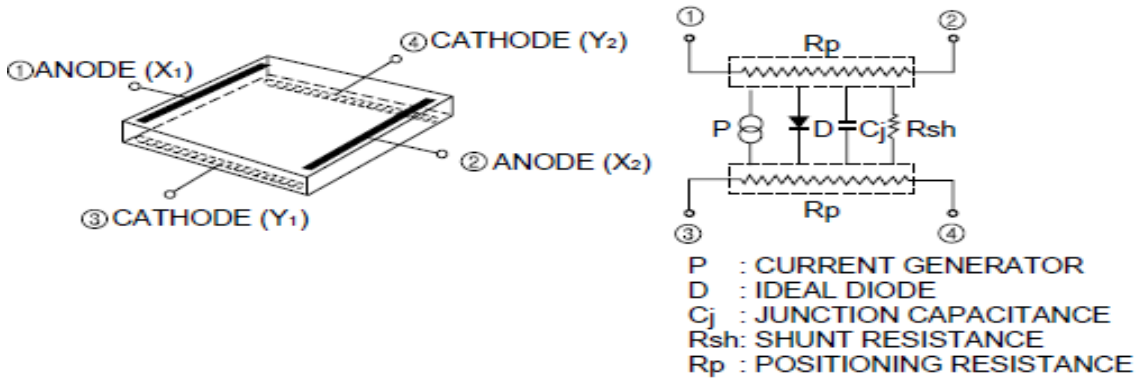

Figure 6.2.4: Structure chart, Equivalent circuit adapted from **[16]**

The light input positions can be calculated from following formulae:

$$\frac{I_{X_2} - I_{X_1}}{I_{X_2} + I_{X_1}} = \frac{2x}{L_X}$$
$$\frac{I_{Y_2} - I_{Y_1}}{I_{Y_2} + I_{Y_1}} = \frac{2y}{L_Y}$$

In the above formula, I_{X_1}, I_{X_2} and I_{Y_1}, I_{Y_2} are the output currents obtained from the electrodes as shown in Figure 6.2.5.

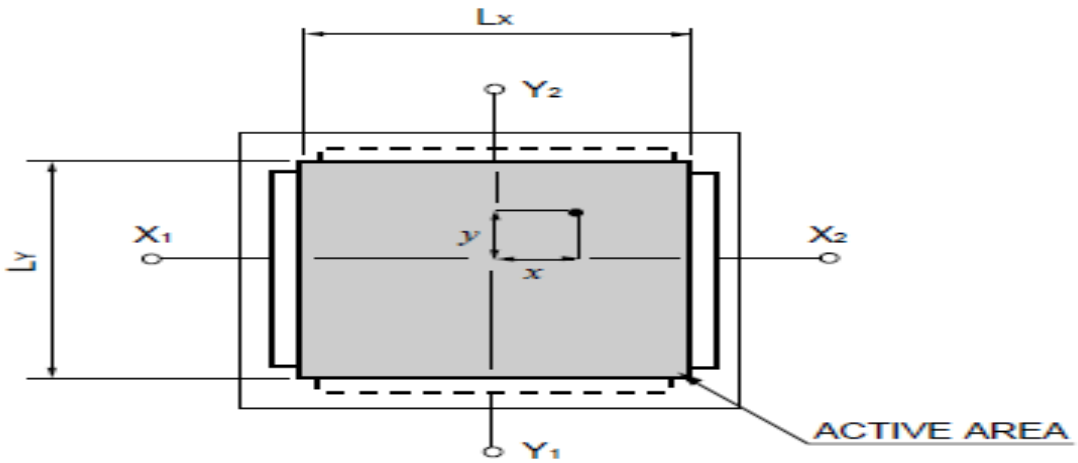

Figure 6.2.5: Active Area Chart adapted from **[16]**

(b) **Tetra-lateral type PSD**

The tetra-lateral type has 4 electrodes on the upper surface, formed along each of the four edges (see Figure 6.2.6). Photocurrent is divided into 4 parts through the same resistive layer and extracted as position signals from the 4 electrodes. Compared to the duo-lateral type, interaction between the electrodes tends to occur near the corners of the active area, making position distortion larger. But the advantages of tetra-lateral type are easy-to-apply reverse bias voltage, small dark current and high-speed response.

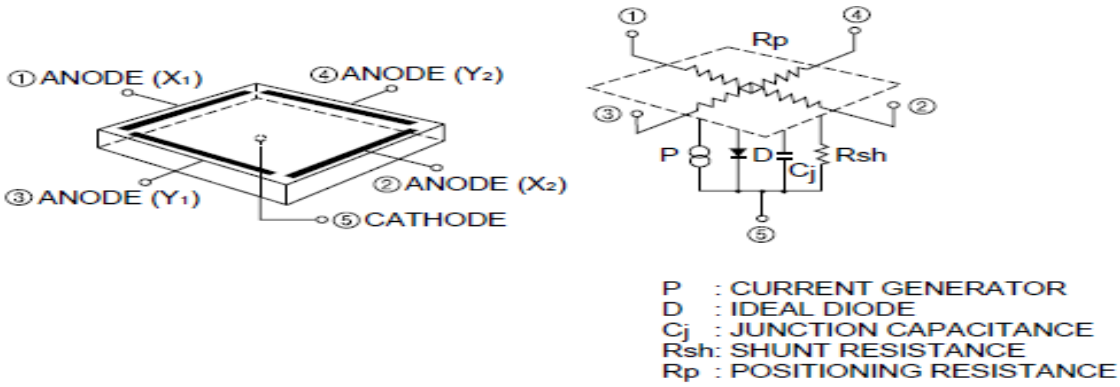

Figure 6.2.6: Structure chart, Equivalent Circuit adapted from **[16]**

The light input position for the tetra-lateral type shown in Figure 6.2.7 is given by following conversion formulae, which are same as for the duo-lateral type.

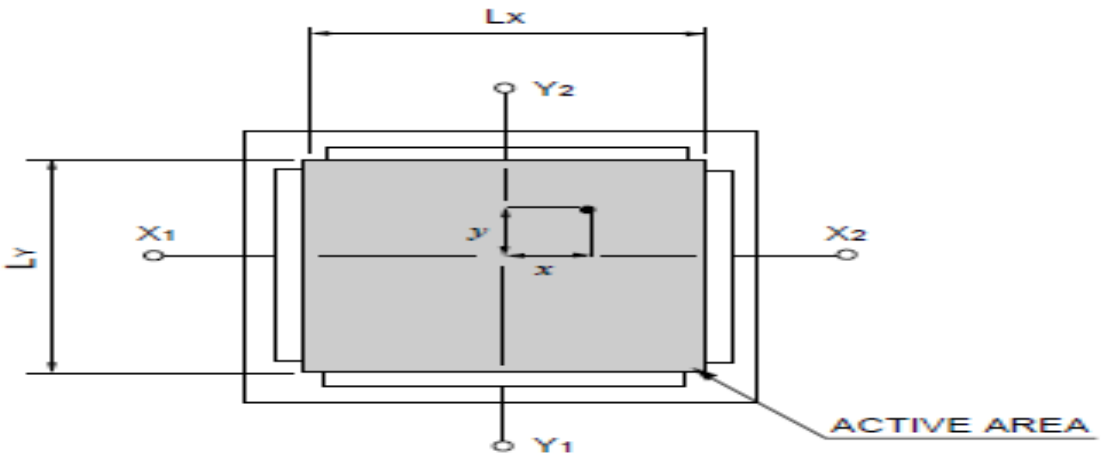

Figure 6.2.7: Active Area Chart adapted from **[16]**

(c) **Pin-cushion Type (Improved Tetra-Lateral Type) PSD**

This is a variant of the tetra-lateral type PSD with an improved active area and reduced interaction between electrodes (see Figure 6.2.8). In addition to the advantages of small dark current, high-speed response and easy application of reverse bias that the tetra-lateral type offers, the circumference distortion has been greatly reduced.

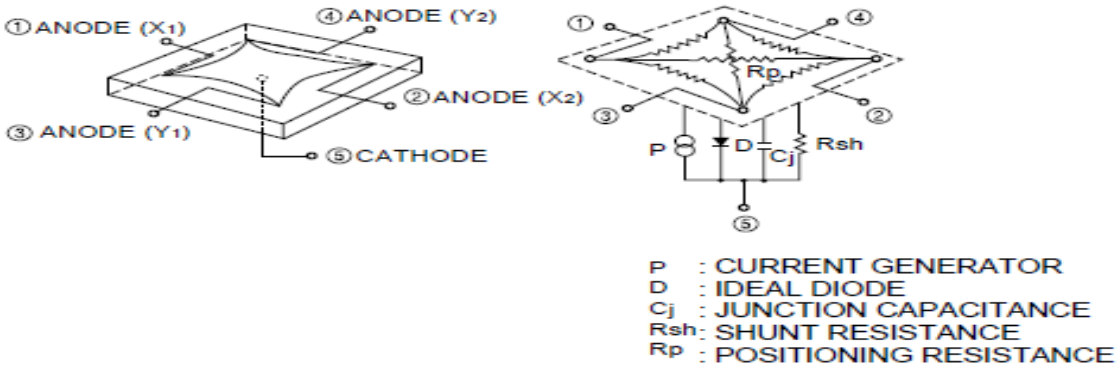

Figure 6.2.8: Structure chart, Equivalent circuit adapted from **[16]**

The light input position of the pin-cushion type shown in Figure 6.2.9 is given by following conversion formulae, which are different from those for the duo-lateral and tetra-lateral types.

$$\frac{(I_{X_2}+I_{Y_1})-(I_{X_1}+I_{Y_2})}{I_{X_1}+I_{X_2}+I_{Y_1}+I_{Y_2}} = \frac{2X}{L_X}$$

$$\frac{(I_{X_2}+I_{Y_2})-(I_{X_1}+I_{Y_1})}{I_{X_1}+I_{X_2}+I_{Y_1}+I_{Y_2}} = \frac{2Y}{L_Y}$$

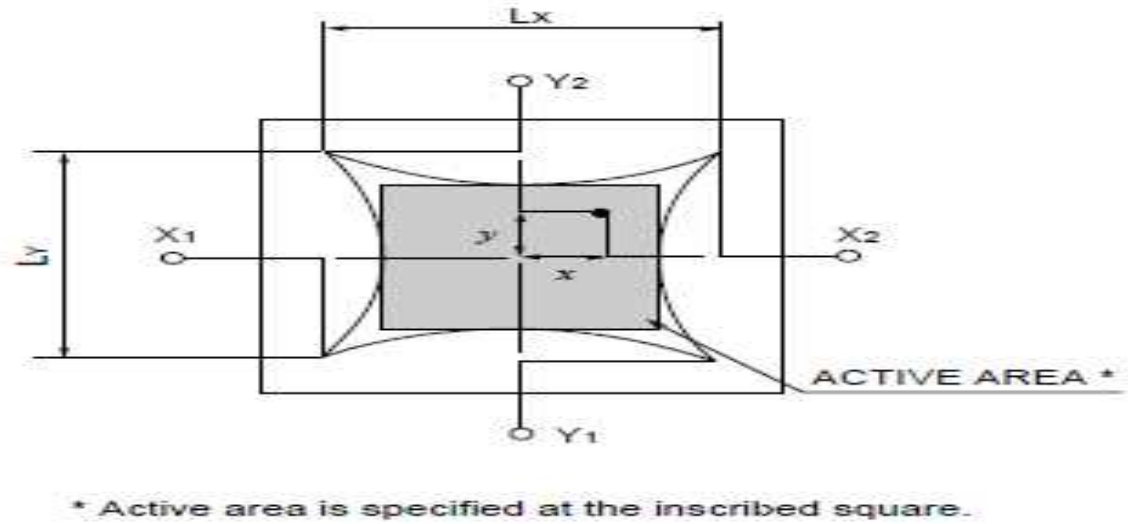

Figure 6.2.9: Active Area Chart adapted from **[16]**

6.3 Kalman Filter

6.3.1 Introduction

Rudolf Emil Kalman was born in Budapest, Hungary, on May 19, 1930. He had the idea of the Kalman filter for the first time in the year 1958. In 1960 and 1961, he published his papers on the Kalman filter and therewith he revolutionized the field of estimation (**[15]**).

Theoretically the Kalman Filter is an estimator for what is called the linear-quadratic problem, which is the problem of estimating the instantaneous "state" of a linear dynamic system perturbed by white noise-by using measurements linearly related to the state but corrupted by white noise. The resulting estimator is statistically optimal with respect to any quadratic function of estimation error.

Practically, it is certainly one of the greatest discoveries in the history of statistical estimation theory and possibly the greatest discovery in the twentieth century. It has enabled humankind to do many things that could not have been done without it, and it has become as indispensable as silicon in the makeup of many electronic systems. Its most immediate applications have been for the control of complex dynamic systems such as continuous manufacturing processes, aircraft, ships, or spacecraft. To control a dynamic system, we must first know what it is doing. For these applications, it is not always possible or desirable to measure every variable that we want to control, and the Kalman filter provides a means for inferring the missing information from indirect (and noisy) measurements. The Kalman filter is also used for predicting the likely future courses of dynamic systems that people are not likely to control, such as the flow of rivers during flood, the trajectories of celestial bodies, etc (**[14]**).

6.3.2 Mathematical Foundation

Figure 6.3.1 depicts the essential subjects forming the foundations for Kalman filtering theory. Although this shows Kalman filtering as the apex of a pyramid, it is itself but part of the foundations of another discipline-"modern" control theory-and a proper subset of statistical decision theory.

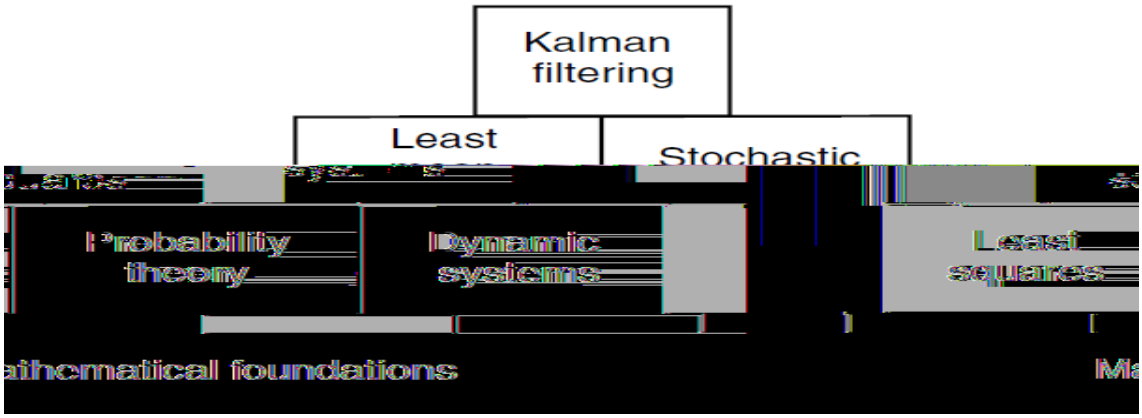

Figure 6.3.1: Foundations of Kalman Filtering adapted from **[14]**

6.3.3 Algorithm

The Kalman filter addresses the general problem of trying to estimate the state $x \in \mathbb{R}^n$ of a discrete-time controlled process that is governed by the linear stochastic difference equation (**[13]**)

$$x_k = Ax_{k-1} + Bu_{k-1} + w_{k-1}$$

with a measurement $z \in \mathbb{R}^m$ i.e

$$z_k = Hx_k + v_k$$

The random variables w and v represent the process and measurement noise (respectively). They are assumed to be independent (of each other), white, and with normal probability distributions

$$
\begin{aligned}
p(w) &\sim N(0,Q) \\
p(v) &\sim N(0,R)
\end{aligned}
$$

In practice, the process noise covariance and measurement noise covariance matrices might change with each time step or measurement, however here we assume they are constant. The $n \times n$ matrix A relates the state at the previous time step $k-1$ to the state at the current step k, in the absence of either a driving function or process noise. Note that in practice A might change with each time step, but here we assume it is constant. The $n \times l$ matrix B relates the optional control input $u \in \mathbb{R}^l$ to the state x . The $m \times n$ matrix H relates the state to the measurement z_k . In practice H might change with each time step or measurement, but here we assume it is constant.

We define $\hat{x}_k^-$ as the apriori state estimation, computed from the previous state estimation $\hat{x}_{k-1}$. The aposteriori state estimation $\hat{x}_k$ corrected based on the measurement z_k. We define the apriori and aposteriori estimate errors as

$$
\begin{aligned}
e_k^- &\equiv x_k - \hat{x}_k^- \\
e_k &\equiv x_k - \hat{x}_k
\end{aligned}
$$

and their covariance

$$
\begin{aligned}
P_k^- &\equiv E\left[e_k^- e_k^{-T}\right] \\
P_k &\equiv E\left[e_k e_k^T\right]
\end{aligned}
$$

Time update and Measurement update equations

The Kalman filter estimates a process by using a form of feedback control: the filter estimates the process state at some time and collects feedback in the form of measurements. As such, the equations for the Kalman filter fall into two groups: time update equations and measurements update equations.

Figure 6.3.2 shows the cycle a kalman filter follows

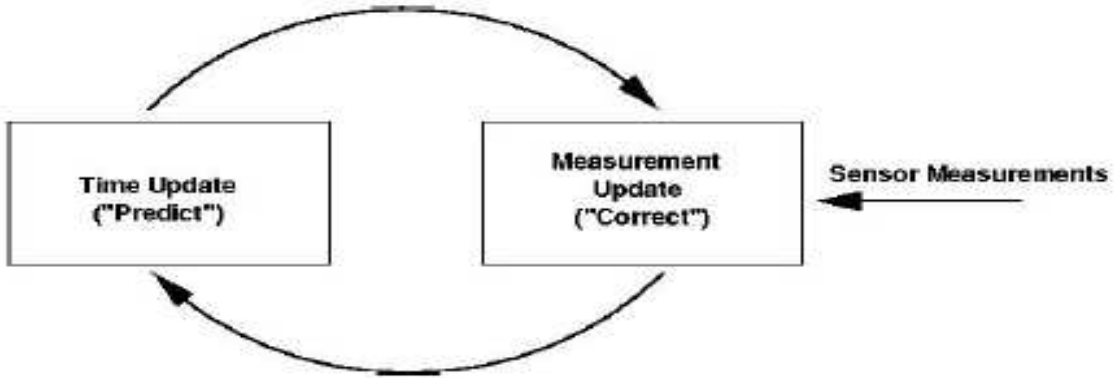

Figure 6.3.2: Kalman Filter Cycle adapted from **[13]**

The apriori state estimate and covariance is obtained by the time update equations as

$$\begin{aligned} \hat{x}_k^- &= A\hat{x}_{k-1} + Bu_k \\ P_k^- &= AP_{k-1}A^T + Q \end{aligned}$$

The aposteriori state estimate and covariance is provided by the measurement update equations as

$$\begin{aligned} K_k &= P_k^- H^T \left(HP_k^- H^T + R\right)^{-1} \\ \hat{x}_k &= \hat{x}_k^- + K_k \left(z_k - H\hat{x}_k^-\right) \\ P_k &= (I - KH) P_k^- \end{aligned}$$

The first task during the measurement update is to compute the Kalman gain, K_k. The next step is to actually measure the process to obtain z_k and then to generate an aposteriori state estimate by incorporating the measurement. The final step is to obtain an aposteriori error covariance estimate P_k.

CHAPTER 7

APPLICATION OF KALMAN FILTERING

The sun sensor is designed to determine the position of the sun in sensor elevation and azimuth coordinates. It consists of a lateral effects sensor (LES) located at the focal plane of the system of lenses that capture the incoming sun light rays. The LES functions as a two-dimensional photo diode designed to locate the position of focused light on the detector surface. The position of the focused light is a function of the elevation and the azimuth angles of the sun. The distances of the focused light from the four corners of the LES are measured, and the position coordinates of the focused light in the LES reference frame is computed. The elevation and azimuth angles of the sun can be computed by following formulae (see Figure 7.0.3):

$$\begin{aligned} Azimuth\,angle, \phi &= \arctan(\frac{y}{x}) \\ Elevation\,angle, \theta &= \arctan(\frac{\sqrt{x^2+y^2}}{h}) \end{aligned}$$

The issue to be considered while determining x and y position coordinates is that the relation between the x-y position coordinates of the focused light and the measured distances is non-linear. To overcome the problem of nonlinearity, intermediate measurements, termed pseudo-measurements, are generated. The pseudo-measurements are some nonlinear function of the measured distances from the focused light where the

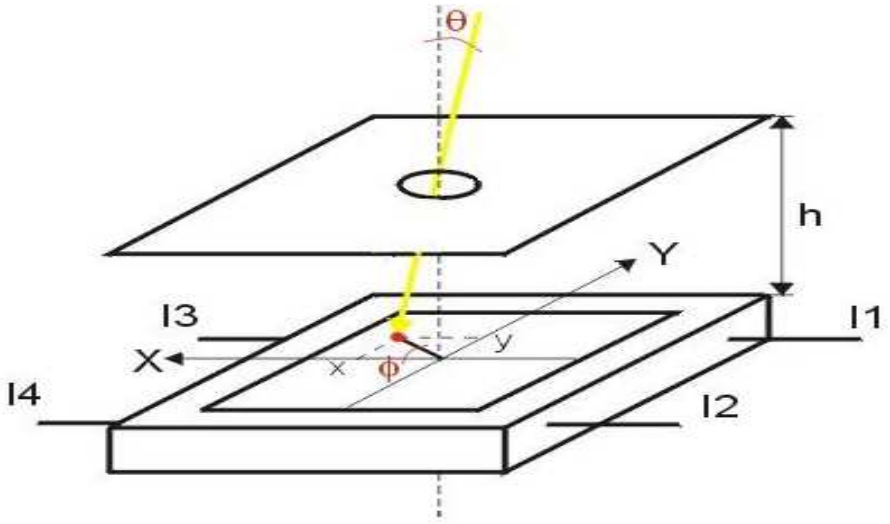

Figure 7.0.3: Angle measurement in PSD adapted from **[5]**

nonlinear function is chosen such that the relation governing the position coordinates and the pseudo-measurements is linear.

7.1 Pseudo-Measurements

Sometimes, the measurements taken might not be linearly or directly related to the x-y position coordinates. Kalman filtering can be used only if the relation is linear in nature. To overcome the problem of nonlinearity, intermediate measurements, termed pseudo-measurements, are generated. The pseudo-measurements are some function of the actual measurements such that the relation governing the position coordinates and the pseudo-measurements is linear (**[4]**).

7.1.1 Tetra-lateral type sun sensor

The current equations for this type of sensor are:

$$\begin{aligned} \frac{I_{X_2} - I_{X_1}}{I_{X_2} + I_{X_1}} &= \frac{2x_R}{L_X} \\ \frac{I_{Y_2} - I_{Y_1}}{I_{Y_2} + I_{Y_1}} &= \frac{2y_R}{L_Y} \end{aligned}$$

Assumptions

- Total current is constant

$$I_{X_1} + I_{X_2} + I_{Y_1} + I_{Y_2} = I_{tot} = constant$$

- Also

$$I_{X_1} + I_{X_2} = k \cdot I_{tot} \quad ; \quad I_{Y_1} + I_{Y_2} = (1-k) \cdot I_{tot} \quad where\, 0 < k < 1$$

Here the actual measurements would be $I_{X_1}, I_{X_2}, I_{Y_1}, I_{Y_2}$. But the pseudo-measurements which we would use are

$$\begin{aligned} y_1 &= I_{X_2} - I_{X_1} = \frac{2k \cdot I_{tot}}{L_x} \cdot x_R \\ y_2 &= I_{Y_2} - I_{Y_1} = \frac{2(1-k) \cdot I_{tot}}{L_y} \cdot y_R \end{aligned}$$

Thus the pseudo-measurement vector is given as

$$\begin{aligned} y &= \begin{bmatrix} y_1 \\ y_2 \end{bmatrix} = \begin{bmatrix} \frac{2k \cdot I_{tot}}{L_x} & 0 \\ 0 & \frac{2(1-k) \cdot I_{tot}}{L_y} \end{bmatrix} \begin{bmatrix} x_R \\ y_R \end{bmatrix} \\ \Rightarrow y &= Gp \end{aligned}$$

where

$$G = \begin{bmatrix} \frac{2k \cdot I_{tot}}{L_x} & 0 \\ 0 & \frac{2(1-k) \cdot I_{tot}}{L_y} \end{bmatrix} \quad ; \quad p = \begin{bmatrix} x_R \\ y_R \end{bmatrix}$$

7.1.2 Pin-cushion type sun sensor

The current equations for this type of sun sensor are:

$$\begin{aligned} \frac{(I_{X_2} + I_{Y_1}) - (I_{X_1} + I_{Y_2})}{I_{X_1} + I_{X_2} + I_{Y_1} + I_{Y_2}} &= \frac{2x_R}{L_X} \\ \frac{(I_{X_2} + I_{Y_2}) - (I_{X_1} + I_{Y_1})}{I_{X_1} + I_{X_2} + I_{Y_1} + I_{Y_2}} &= \frac{2y_R}{L_Y} \end{aligned}$$

Assumption

- Total current is constant

$$I_{X_1} + I_{X_2} + I_{Y_1} + I_{Y_2} = I_{tot} = constant$$

Here the actual measurements would be $I_{X_1}, I_{X_2}, I_{Y_1}, I_{Y_2}$. But the pseudo measurements which we would use are

$$\begin{aligned} y_1 &= (I_{X_2} + I_{Y_1}) - (I_{X_1} + I_{Y_2}) = \frac{2I_{tot}}{L_x} \cdot x_R \\ y_2 &= (I_{X_2} + I_{Y_2}) - (I_{X_1} + I_{Y_1}) = \frac{2I_{tot}}{L_y} \cdot y_R \end{aligned}$$

Thus the pseudo-measurement vector is given as

$$\begin{aligned} y &= \begin{bmatrix} y_1 \\ y_2 \end{bmatrix} = \begin{bmatrix} \frac{2I_{tot}}{L_x} & 0 \\ 0 & \frac{2I_{tot}}{L_y} \end{bmatrix} \begin{bmatrix} x_R \\ y_R \end{bmatrix} \\ \Rightarrow y &= Gp \end{aligned}$$

where

$$G = \begin{bmatrix} \frac{2I_{tot}}{L_x} & 0 \\ 0 & \frac{2I_{tot}}{L_y} \end{bmatrix} \quad ; \quad p = \begin{bmatrix} x_R \\ y_R \end{bmatrix}$$

7.2 State Space Model

The actual pseudo-measurement 'y' will be subject to errors. The discrepancy between the true and the actual pseudo-measurement is due to the atmospheric conditions such as moving clouds and other measurement errors.Thus

$$y = Gp + \nu$$

where v is the error

$$v = \begin{bmatrix} v_1 \\ v_2 \end{bmatrix}$$

7.2.1 Model for the evolution of the Sun Position

The state-space model governing the evolution of the sun position takes the following form (**[4]**):

$$\begin{aligned} x(k+1) &= Ax(k) + Bw(k) \\ p(k) &= Cx(k) \end{aligned}$$

where x is the state

w is the zero-mean white noise process.

If the sun position remains essentially constant over the interval of observation, then the state $x = p$ and $A = I$ implies that the state—namely, the position of the focused light p —is essentially constant (mean of x is constant). If, however, the time interval of measurement is large, the sun position, and hence p, will vary; the state x in general will include not only the position p but also its derivatives, $p^{(i)}, i = 1,2,\ldots\ldots$ where $p^{(i)}$ is the i^{th} derivative of p. Assuming a parabolic approximation to the trajectory, the state x will include the position p and the first and second derivatives of p. The state x and the matrices A and B take the form

$$x = \begin{bmatrix} x_R \\ \dot{x_R} \\ \ddot{x_R} \\ y_R \\ \dot{y_R} \\ \ddot{y_R} \end{bmatrix}$$

$$A = \begin{bmatrix} 1 & 1 & 1 & 0 & 0 & 0 \\ 0 & 1 & 1 & 0 & 0 & 0 \\ 0 & 0 & 1 & 0 & 0 & 0 \\ 0 & 0 & 0 & 1 & 1 & 1 \\ 0 & 0 & 0 & 0 & 1 & 1 \\ 0 & 0 & 0 & 0 & 0 & 1 \end{bmatrix} \qquad B = \begin{bmatrix} 0.1667 & 0 \\ 0.5 & 0 \\ 1 & 0 \\ 0 & 0.1667 \\ 0 & 0.5 \\ 0 & 1 \end{bmatrix} \qquad C = \begin{bmatrix} 1 & 0 & 0 & 0 & 0 & 0 \\ 0 & 0 & 0 & 1 & 0 & 0 \end{bmatrix}$$

If the plant noise w is absent i.e if $w = 0$ then the above equation implies merely that the position and the state are deterministic.

The state space model relating the pseudo-measurement y and the state x may be derived from the above by merely including the measurement noise as follows:

$$\begin{aligned} x(k+1) &= Ax(k) + Bw(k) \\ y(k) &= Hx(k) + \vartheta(k) \end{aligned}$$

where ϑ is the measurement error which is considered as a random noise and

$$H = GC$$

This model when passed through the 5 stages of the iterative Kalman filter algorithm would yield the robust estimate of the position coordinates of the sun.

7.3 Estimation using Algebraic Model

The position estimate of the sun $p = [x_R \quad y_R]^T$ can also be obtained by solving the linear least squares problem (**[4]**).

The optimal estimate $\hat{p} = [\hat{x_R} \quad \hat{y_R}]^T$ is determined from

$$\min_{\hat{p}} \left\{ (y - G\hat{p})^T (y - G\hat{p}) \right\}$$

Solving this, we get

$$\hat{p} = G^{\dagger} y$$

where $G^{\dagger}$ is the pseudo-inverse of G given by

$$G^{\dagger} = \left(G^T G\right)^{-1} G^T$$

As the matrix G we got for both sun sensors is an invertible square matrix of the form $\begin{bmatrix} a & 0 \\ 0 & b \end{bmatrix}$, hence

$$G^{\dagger} = G^{-1} = \begin{bmatrix} \frac{1}{a} & 0 \\ 0 & \frac{1}{b} \end{bmatrix}$$

Thus the position coordinates we would get using this algebraic method is given by

$$\hat{p} = \begin{bmatrix} \hat{x_R} \\ \hat{y_R} \end{bmatrix} = \begin{bmatrix} \frac{y_1}{a} \\ \frac{y_2}{b} \end{bmatrix}$$

CHAPTER 8

SIMULATION RESULTS AND DISCUSSION

8.1 Simulation Environment

Table 8.1.1 explains the simulation environment under which simulations were carried out.

Parameter	**Specification**
Sun Sensors	Tetra-lateral type Pin-cushion type
Sampling Time	0.1sec
Total duration of run	100 sec
Plant noise standard deviation	0.05
Measurement noise standard deviation	3
Distance between two electrodes, $L_x = L_y = L$	10 mm
Total Current, I_{tot}	$200\,\mu A$

Table 8.1.1: Simulation Parameters

8.2 Simulation Results

8.2.1 Pin-cushion type sun sensor

Figure 8.2.1 gives a basic view of a pin-cushion type sun sensor.

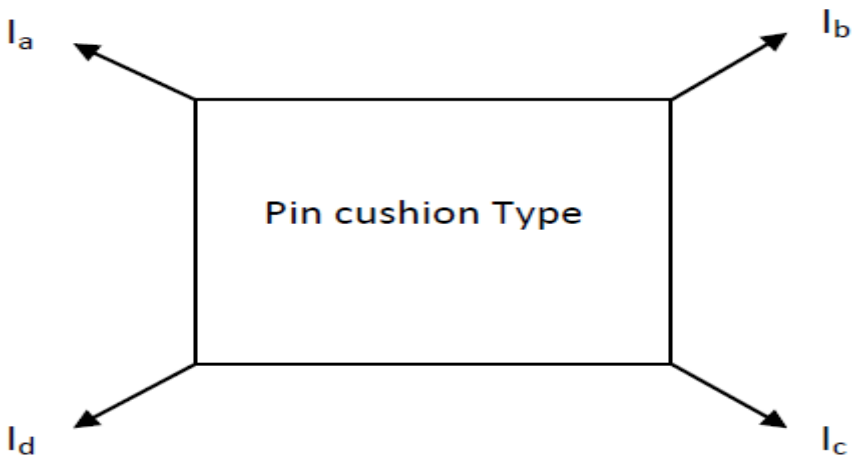

Figure 8.2.1: View of pin-cushion type sun sensor

Here currents I_a, I_b, I_c, I_d correspond to the four currents from four corners of the pin cushion type sun sensor. They satisfy the following current equations

$$\begin{aligned} \frac{(I_c+I_b)-(I_a+I_d)}{I_a+I_b+I_c+I_d} &= \frac{2x_R}{L} \\ \frac{(I_c+I_d)-(I_a+I_b)}{I_a+I_b+I_c+I_d} &= \frac{2y_R}{L} \end{aligned}$$

Figure 8.2.2 shows the estimated x and y positions of the sun using Kalman Filter and Algebraic method. The true values of x and y were also shown.

The actual x and y positions are

$$x = -1.25\,mm \qquad y = 2.25\,mm$$

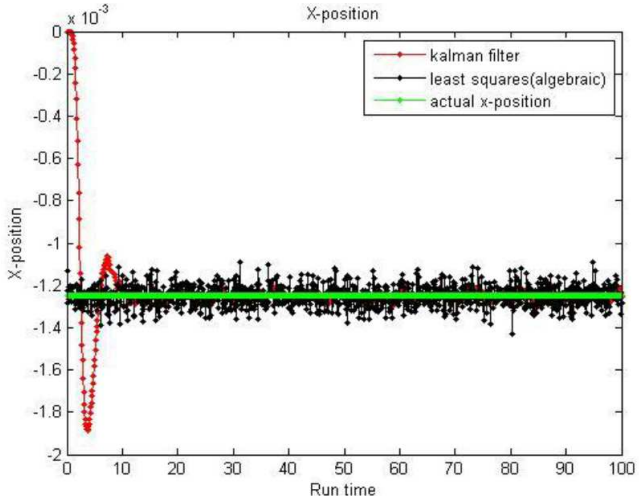

(a) X-position estimation

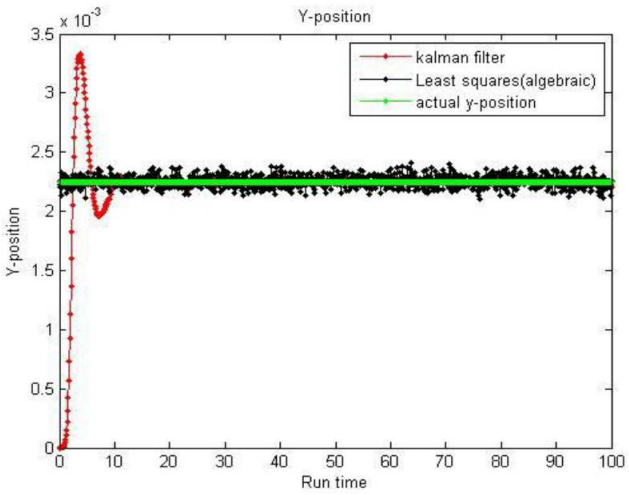

(b) Y-position estimation

Figure 8.2.2: $\mathbf{I_a = 30\mu A}$, $\mathbf{I_b = 25\mu A}$, $\mathbf{I_c = 50\mu A}$, $\mathbf{I_d = 95\mu A}$. Figure shows the true values, kalman filter estimates and algebraic method estimates of the x and y position

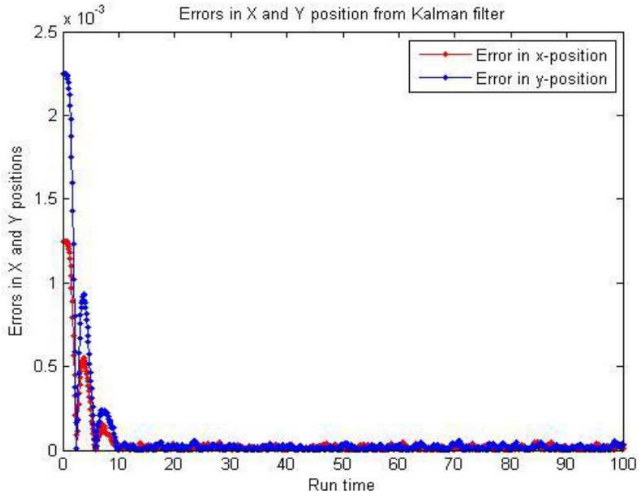

(a) Errors in Kalman Filtering

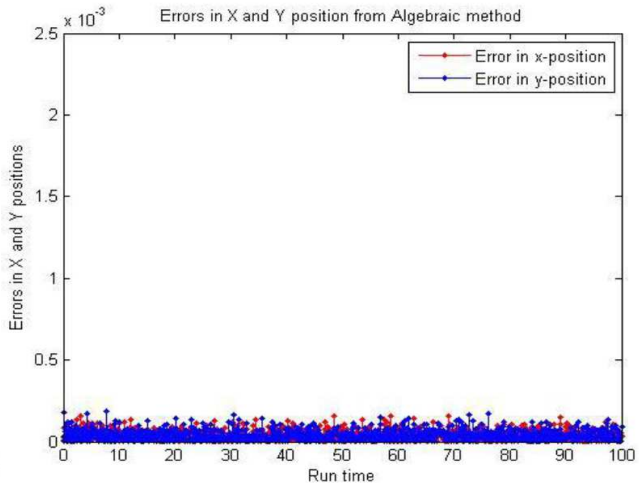

(b) Errors in Algebraic method

Figure 8.2.3: $\mathbf{I_a = 30\mu A}$, $\mathbf{I_b = 25\mu A}$, $\mathbf{I_c = 50\mu A}$, $\mathbf{I_d = 95\mu A}$. Figure shows the errors in x and y positions in kalman filtering and algebraic method

From the Figure 8.2.3, the following conclusion can be made

- Standard deviations of the position coordinates using Kalman filter are

$$\sigma_x = 0.020\,mm \qquad \sigma_y = 0.018\,mm$$

- Standard deviation of the position coordinates using Algebraic method are

$$\sigma_x = 0.049\,mm \qquad \sigma_y = 0.048\,mm$$

8.2.2 Tetra-lateral type sun sensor

Figure 8.2.4 gives a basic view of a tetra-lateral type sun sensor

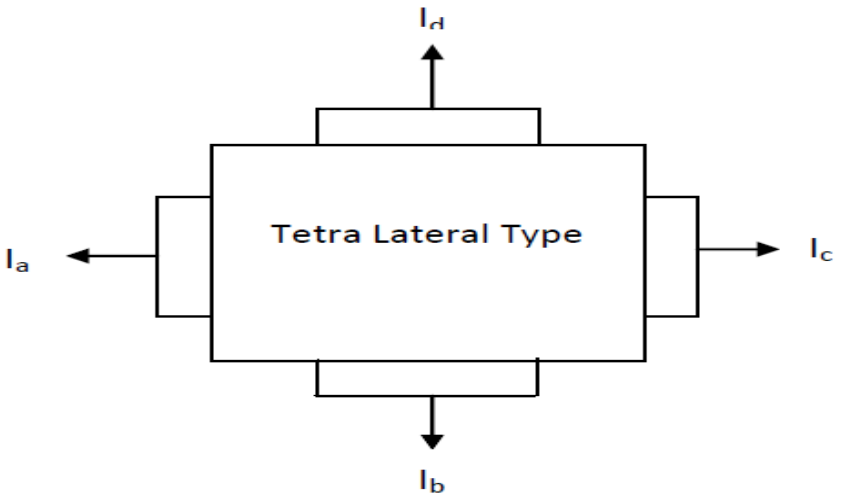

Figure 8.2.4: View of Tetra-lateral type sun sensor

Here currents I_a, I_b, I_c, I_d correspond to the four currents from four corners of the tetra-lateral type sun sensor. They satisfy the following current equations

$$\begin{aligned} \frac{I_c - I_a}{I_a + I_c} &= \frac{2x_R}{L} \\ \frac{I_d - I_b}{I_b + I_d} &= \frac{2y_R}{L} \end{aligned}$$

Figure 8.2.5 shows the estimated x and y positions of the sun using Kalman Filter and Algebraic method. The true values of x and y were also shown.

The actual x and y positions are

$$x = 2\,mm \qquad y = 2.5\,mm$$

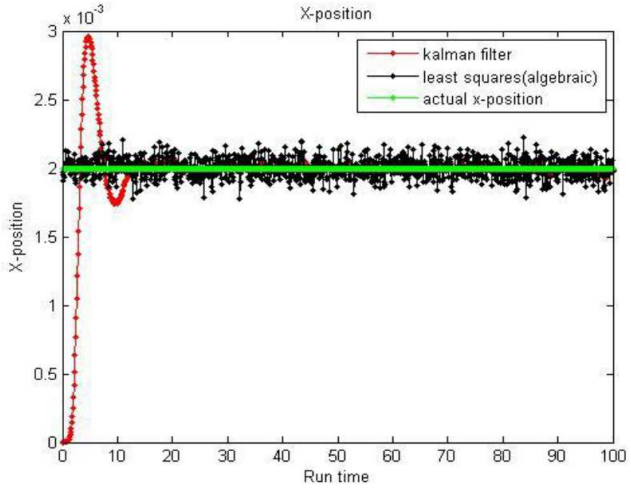

(a) X-position estimation

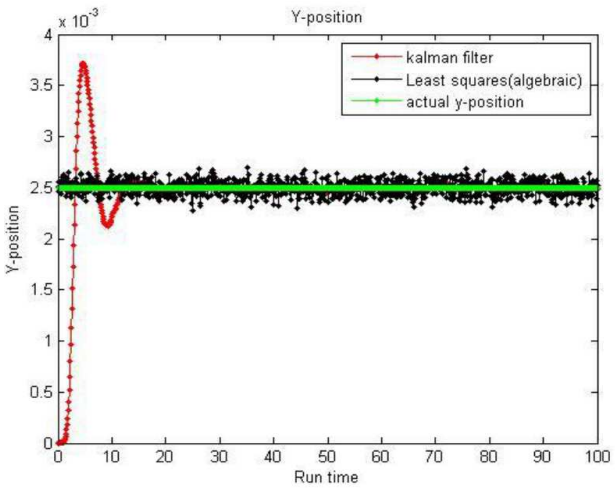

(b) Y-position estimation

Figure 8.2.5: $\mathbf{I_a = 30\mu A}$, $\mathbf{I_b = 25\mu A}$, $\mathbf{I_c = 70\mu A}$, $\mathbf{I_d = 75\mu A}$. Figure shows the true values, kalman filter estimates and algebraic method estimates of the x and y position

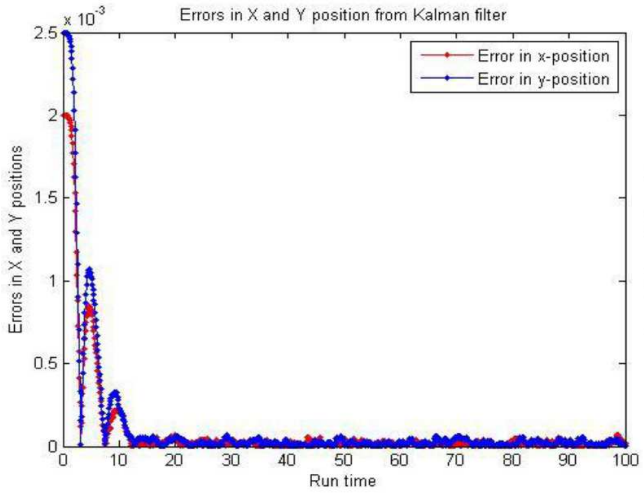

(a) Errors in Kalman Filtering

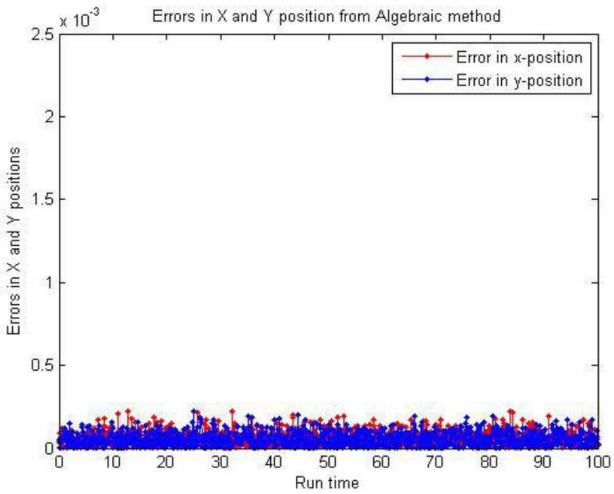

(b) Errors in Algebraic method

Figure 8.2.6: $\mathbf{I_a = 30\mu A}$, $\mathbf{I_b = 25\mu A}$, $\mathbf{I_c = 70\mu A}$, $\mathbf{I_d = 75\mu A}$. Figure shows the errors in x and y positions in kalman filtering and algebraic method

From the Figure 8.2.6, the following conclusion can be made

- Standard deviations of the position coordinates using Kalman filter are

$$\sigma_x = 0.023\,mm \qquad \sigma_y = 0.023\,mm$$

- Standard deviation of the position coordinates using Algebraic method are

$$\sigma_x = 0.072\,mm \qquad \sigma_y = 0.073\,mm$$

CHAPTER 9

CONCLUSIONS AND FUTURE SCOPE

9.1 Receiver Algorithm

9.1.1 Conclusion

Performance of a LTE system is often limited by the presence of various sources of interference, hence leading to IOSI, IBI, CAI, CCI. In addition, OFDM, a multi-carrier modulation technique with great promise to cater next millennia data needs and a potential candidate in the evolution of 4G technology, is highly sensitive to frequency offset (ICI). Discrepancy in percentage of carrier frequency offset, however minor it might be, leads to significant degradation in SNR, thereby resulting in reduced system performance. To compensate all such effects, Robert Heath proposed Channel-Shortening technique. This solution makes use of space-time equalizer, but is limited by a constraint that total active receive antennas should be greater than total active transmit antennas.

Practically, implementing large number of receive antennas at the mobile terminal is not realistic. Hence a technique is proposed in this project that furnishes all the merits offered by Channel-Shortening method and without limitation on number of receive antennas. This method is simulated and tested for different cases. A parameter 'Diversity' is used to contrast the two techniques under contention.

Results hence obtained are depicted below.

In the absence of frequency offset, the Proposed method is observed to provide diversity improvement by a factor of 2 (approximately). Same has been concluded for equal frequency offset (between all base station-receiver pairs). However, in the presence of unequal frequency offsets, diversity improvement was found to be atmost 2 but atleast greater than 1. Therefore, the worst case scenario would be equal transmit and receive antennas for the Proposed method. Hence, even the worst case scenario of Proposed method offers better performance than Channel-Shortening method, in its best scenario. Cherry in the Cake is that bit rate was not sacrificed in due process.

9.1.2 Future Scope

This project can be extended in following areas:

1. It is observed from the simulations that BER of the Proposed method is relatively higher than the non-compensated case till a specific SNR value, called the 'cross-over' point. Beyond this point, Proposed method proves to be more beneficial in regards to BER, however at the cost of increased complexity. Therefore, in the future prospects, one can aim at designing a hybrid scheme, which uses the conventional non-compensated technique till the cross-over and then switch to the proposed method thereafter. This system is expected to show improved performance with reduced complexity, atleast till the cross-over.
2. Further, this project was limited to studying application of proposed method to downlink scenario alone. Hence, it can be extended to LTE Uplink (SC-FDMA) systems also.
3. Also, Coded performance will be better than the uncoded ones. Hence one can extend this project for coded case and credibility of the proposed method can be tested in this picture as well.

9.2 Kalman Filter Algorithm

9.2.1 Conclusion

In this project, the Kalman filtering algorithm was simulated and applied to the unfiltered output of 2 types of sun sensors namely Tetra-lateral and Pin-cushion type. Robust position estimate of the sun was hence determined. Simulations prove that the estimated position is appropriate even in the presence of multiple noise sources that corrupt the sensor measurements. The results are compared with algebraic method to show the superiority of Kalman Filtering.

A major noise source that adversely affect the sensor measurements is Earth's Albedo flux. However, by designing the Field of View (FOV) of the sun sensor to be within some predetermined limits, the discrepancies introduced by Albedo flux become trivial (**[12]**). This assumption has been considered while developing the algorithm in the present project.

Table 9.2.1 presents a comparative study between Kalman filter and Algebraic method in terms of maximum deviation in output data.

	Pin Cushion		**Tetra Lateral**	
	X	**Y**	**X**	**Y**
Kalman filter	0.020mm	0.018mm	0.023mm	0.023mm
Algebraic method	0.049mm	0.048mm	0.072mm	0.073mm

Table 9.2.1: Comparison of the standard deviation of both methods

From the above results, it is evident that standard deviations of Kalman filter are less than half that are exhibited by the conventional algebraic method. Therefore, it provides extraordinary filtering when compared to other filters and hence, gives most appropriate estimate of sun's position even in the presence of corrupted output from sun sensors.

9.2.2 Future Scope

While designing the algorithm for Kalman filter it is assumed that the effect of Albedo flux is negligible once FOV is restricted to a specific range. Being a major source of noise that taints position estimate of the sun, it becomes important to study the limitation of such an assumption. However, scenario when this assumption fails is not ventured in this project. Hence, as a future prospect, one can study the behaviour of Kalman filter in the presence of significant Earth's Albedo Flux.

REFERENCES

[1] **Robert W. Heath** and **Taiwen Tang**, *Space-Time Interference Cancellation in MIMO-OFDM Systems,* IEEE Transactions on Vehicular Technology, Vol. 54, No. 5, September 2005, **1802-1816**.

[2] **K. Giridhar, Istdeo Singh,** *Interference Mitigation using Channel Shortening Pre-filter for SIMO-OFDM Systems,* 2013 IEEE 14th Workshop on Signal Processing Advances in Wireless Communications (SPAWC).

[3] **Robert W. Heath** and **Taiwen Tang**, *A Space–Time Receiver With Joint Synchronization and Interference Cancellation in Asynchronous MIMO-OFDM Systems*, IEEE Transactions on Vehicular Technology, Vol. 57, No. 5, September 2008, **2991-3005**.

[4] **R. DoraiSwami** and **R. Stephen Price**, *A Robust Position Estimation Scheme Using Sun Sensor*, IEEE Transactions on Instrumentation and Measurement, Vol. 47, No. 2,April 1998, **595-603**.

[5] **Pedro M. Rodrigues, Pedro M. Ramos**, *Design and Characterization of a Sun Sensor for the SSETI-ESEO Project*, XVIII IMEKO WORLD CONGRESS Metrologyfor a Sustainable Development, September 17 – 22, 2006, Rio de Janeiro, Brazil.

[6] **Kiran Kumar Kuchi**, *Generalization of Widely Linear Filtering Concepts for Equalization and Interference Suppression in PAM/QAM Systems*, Phd Thesis, 2006.

[7] **Bernard Picinbono** and **Pascal Chevalier**, *Widely Linear Estimation with Complex Data*, IEEE Transactions on Signal Processing, Vol. 43, No. 8, August 1995, **2030-2033**.

[8] **Prof Aditya. K. Jagannatham**, IIT Kanpur, *Advanced 3G and 4G Wireless Mobile Communications*, NPTEL Video Lecture.

[9] **Ankit Ashok Agarwal**, *Pilot based channel estimation for 3GPP LTE Downlink*, MS thesis, University of Texas at Arlington, December 2011.

[10] **Robert W. Heath, Roopsha Samanta** and **Brian L. Evans**, *Joint Interference Cancellation and Channel Shortening in Multiuser-MIMO Systems*, IEEE Transactions on Vehicular Technology, Vol. 56, No. 2, March 2007, **652-660**.

[11] **Yonatan Winetraub, San Bitan** and **Uval dd Dr Anna B. Heller**, *Attitude Determination-Advanced Sun sensors for Pico Satellites*, Handasaim School, Tel-Aviv University, Israel.

[12] **Robert Valner**, *Characterization of Custom Built Sun Sensors for ESTCube-1*, Bachelor's Thesis, University of Tartu, Faculty of Science and Technology, Institute of Physics.

[13] **Greg Welch** and **Gary Bishop**, *An Introduction to the Kalman Filter*, UNC-Chapel Hill, TR 95-041, July 24, 2006.

[14] **Mohinder S. Grewal** and **Angus P. Andrews**, *Kalman Filtering: Theory and Practice using MATLAB*, 2nd edition, A Wiley-Interscience Publication, John Wiley & Sons,Inc., 2001, **11-20**.

[15] **Rachel Kleinbauer**, *Kalman Filtering Implementation with MATLAB*, Study Report in the Field of Study GeoDesy and GeoInformatics, Universitat Stuttgart, Helsinki, November 2004.

[16] *2D PSD Characteristics & Use*, **URL**: http://www.hamamatsu.com/resources/pdf/ssd.

[17] *LTE Evolution and Specifications*, **URL**: www.tutorialspoint.com/lte.

[18] *LTE Parameters*, **URL**: www.radio-electronics.com/info/cellulartelecomms/lte-longterm-evolution.

[19] *About LTE*, **URL**: en.wikipedia.org/wiki/LTE_(telecommunications)